



---

Masters Theses

Graduate School

---

8-1960

## Effect of alloying additions on corrosion behavior of nickel-molybdenum alloys in fused fluoride mixtures.

Jackson Harvey DeVan  
*University of Tennessee*

---

Follow this and additional works at: [https://trace.tennessee.edu/utk\\_gradthes](https://trace.tennessee.edu/utk_gradthes)

---

### Recommended Citation

DeVan, Jackson Harvey, "Effect of alloying additions on corrosion behavior of nickel-molybdenum alloys in fused fluoride mixtures.. " Master's Thesis, University of Tennessee, 1960.  
[https://trace.tennessee.edu/utk\\_gradthes/5784](https://trace.tennessee.edu/utk_gradthes/5784)

To the Graduate Council:

I am submitting herewith a thesis written by Jackson Harvey DeVan entitled "Effect of alloying additions on corrosion behavior of nickel-molybdenum alloys in fused fluoride mixtures.." I have examined the final electronic copy of this thesis for form and content and recommend that it be accepted in partial fulfillment of the requirements for the degree of Master of Science, with a major in Metallurgical Engineering.

W. O. Harms, Major Professor

We have read this thesis and recommend its acceptance:

Accepted for the Council:

Carolyn R. Hodges

Vice Provost and Dean of the Graduate School

(Original signatures are on file with official student records.)

August 15, 1960

To the Graduate Council:

I am submitting herewith a thesis written by Jackson Harvey DeVan entitled "Effect of Alloying Additions on Corrosion Behavior of Nickel-Molybdenum Alloys in Fused Fluoride Mixtures." I recommend that it be accepted for nine quarter hours of credit in partial fulfillment of the requirements for the degree of Master of Science, with a major in Metallurgical Engineering.

W.O. Farms  
\_\_\_\_\_  
Major Professor

We have read this thesis and  
recommend its acceptance:

J. J. Pasqua  
E. E. Mansbury

Accepted for the Council:

Dale Martens  
\_\_\_\_\_  
Dean of the Graduate School

EFFECT OF ALLOYING ADDITIONS ON CORROSION BEHAVIOR  
OF NICKEL-MOLYBDENUM ALLOYS IN  
FUSED FLUORIDE MIXTURES

---

A Thesis  
Presented to  
the Graduate Council  
University of Tennessee

---

In Partial Fulfillment  
of the Requirements for the Degree  
Master of Science

---

by  
Jackson Harvey DeVan  
August 1960

*24  
33-1*

#### ACKNOWLEDGEMENTS

The author wishes to thank Dr. W. O. Harms for his invaluable comments and contributions to the preparation of this manuscript. He is also indebted to Drs. G. M. Watson and R. B. Evans, III, of the Materials Chemistry Division, who assisted in the design and operation of radiotracer loop experiments.

Chemical analyses required for the interpretation of the present studies were provided by W. F. Vaughan of the ORNL Reactor Projects Analytical Laboratory. Preparation of alloy specimens for metallurgical examination and the photomicrography was done by C. E. Zachary of the Metallurgy Division, ORNL.

Also, the author is indebted to Mrs. W. L. Norton for the typing of this manuscript and to the ORNL Graphic Arts Department for the preparation of drawings included in this report.

470436

## SUMMARY

Fused fluoride mixtures containing  $\text{UF}_4$  have been developed as fuel solutions for high temperature nuclear reactors. The purpose of the present investigation was to evaluate the corrosion properties of alloys composed basically of Ni and Mo for containment of these mixtures. These evaluations utilized thermal convection loops which circulated salt mixtures between a hot-zone temperature of  $815^{\circ}\text{C}$  and a cold-zone temperature of  $650^{\circ}\text{C}$ .

Initial corrosion studies were made with Ni-base alloys containing 17 to 20 per cent Mo and various percentages of Cr, Al, Ti, V, Fe, Nb, and W. Loops of these alloys were exposed to the salt mixture  $\text{NaF-LiF-KF-UF}_4$  (11.2-45.3-41.0-2.5 mole per cent) for periods of 500 and 1000 hours. Measurements of the concentrations of corrosion products in after-test salt samples indicated the corrosion susceptibility of alloying additions to increase in this order: Fe, Nb, V, Cr, W, Ti, and Al. However, metallographic examinations of loop surfaces showed relatively light attack for all alloys except those containing combined additions of Al and Ti or Al and Cr.

A Ni-base alloy containing 17 per cent Mo, 7 per cent Cr, and 5 per cent Fe, designated INOR-8, was found to afford the best combination of strength and corrosion resistance

among the alloy compositions tested and was selected for further corrosion studies. Corrosion of this alloy was found to occur by the selective oxidation of Cr and, accordingly, was controlled by the rate at which Cr diffused to surfaces undergoing attack. To determine these rates, the diffusion coefficients for Cr in INOR-8 were measured over the temperature range 870°C to 680°C by exposing the alloy to a fused fluoride mixture containing radioactive Cr in the form of CrF<sub>2</sub>. The diffusion coefficients were computed from measurements of the intake of radioactive Cr by the alloy and from an analysis of the concentration profile of radioactive Cr below the exposed surfaces of the metal. The magnitudes of the diffusion coefficients ranged from 10<sup>-12</sup> to 10<sup>-14</sup> cm<sup>2</sup>/sec and compared closely to the coefficients determined for Cr in the Ni-base alloys.

To evaluate the validity of these coefficients for the prediction of corrosion rates, a second INOR-8 loop was allowed to absorb radioactive Cr and was then exposed to the corrosive agent FeF<sub>2</sub>. The observed rates of tracer migration closely corresponded to those predicted by the use of the Cr diffusion coefficients determined from the first loop experiment.

In both of the radiotracer loop experiments, the rate of Cr movement in areas farthest removed from the metal-salt interface was governed by higher diffusion coefficients than

tracer nearer the surface. This behavior was attributed to the increased importance of grain-boundary diffusion relative to volume diffusion at higher penetration depths.

The diffusivity data from the radiotracer experiments were applied to calculations of the corrosion rates of INOR-8 effected by fluoride mixtures containing  $\text{UF}_4$ . Boundary conditions assumed for these calculations were that 1) mass transport rates were controlled by the diffusion rate of Cr in the container material, and 2) that Cr surface concentrations were at all times controlled by the concentrations of corrosion products within the salt. These calculations indicated that under prolonged exposure to the salt system  $\text{NaF-ZrF}_4\text{-UF}_4$  (50-46-4 mole per cent) circulating between  $800^{\circ}\text{C}$  and  $600^{\circ}\text{C}$ , the Cr concentration of INOR-8 would not be reduced below a level of 3.5 per cent. Accordingly, the maximum corrosion rates for the alloy in this system were found to be relatively small.

## TABLE OF CONTENTS

CHAPTER	PAGE
I. INTRODUCTION . . . . .	1
II. OBJECTIVES . . . . .	4
III. REVIEW OF RELATED WORK . . . . .	5
Corrosion by Fluoride Mixtures . . . . .	5
Corrosion Reactions . . . . .	5
Reduction of UF <sub>4</sub> by Cr . . . . .	6
Corrosion of Ni-Mo Alloys . . . . .	10
IV. MATERIALS AND PROCEDURES . . . . .	13
Effects of Alloying Additions . . . . .	13
Test Materials . . . . .	13
Test Equipment . . . . .	14
Salt Preparation . . . . .	20
Operating Procedures . . . . .	22
Test Examination . . . . .	24
Metallographic Examination . . . . .	25
Chemical Analyses . . . . .	25
Radiotracer Techniques . . . . .	26
Chromium Tracer . . . . .	27
Molten Fluoride Solvent . . . . .	27
Counting Techniques . . . . .	27
Test Apparatus . . . . .	28
Operating Procedure . . . . .	28

CHAPTER	PAGE
Test Analysis . . . . .	32
Corrosion Experiment (Loop 1249) . . . . .	33
V. RESULTS AND DISCUSSION . . . . .	35
Effects of Alloying Additions . . . . .	35
Chromium . . . . .	35
Corrosion-Product Concentrations . . . . .	35
Metallographic Results . . . . .	43
Aluminum . . . . .	44
Corrosion-Product Concentrations . . . . .	44
Metallographic Results . . . . .	51
Titanium . . . . .	53
Corrosion-Product Concentrations . . . . .	53
Metallographic Results . . . . .	53
Vanadium . . . . .	56
Corrosion-Product Concentrations . . . . .	56
Metallographic Results . . . . .	56
Iron . . . . .	58
Corrosion-Product Concentrations . . . . .	58
Metallographic Results . . . . .	58
Niobium . . . . .	60
Corrosion-Product Concentrations . . . . .	60
Metallographic Results . . . . .	60
Tungsten . . . . .	64
Corrosion-Product Concentrations . . . . .	64

CHAPTER	PAGE
Metallographic Results . . . . .	64
Relative Thermodynamic Stabilities of Alloying Constituents . . . . .	67
General Discussion of Alloying Effects . . .	69
Corrosion Properties of INOR-8 . . . . .	74
Radiotracer Diffusion Experiment (Loop 1248) .	75
Diffusivity Measurements . . . . .	75
Significance of Diffusion Coefficients . . .	79
Radiotracer Corrosion Experiment (Loop 1249) .	82
Diffusivity Measurements . . . . .	84
Corrosion Rates . . . . .	88
Corrosion of INOR-8 by UF <sub>4</sub> . . . . .	94
Cr Mass Transfer by UF <sub>4</sub> -Containing Salts .	94
Calculation of Corrosion Rates . . . . .	96
VI. CONCLUSIONS AND RECOMMENDATIONS . . . . .	103
Conclusions . . . . .	103
Recommendations . . . . .	105
LIST OF REFERENCES . . . . .	107
APPENDICES . . . . .	110
A. Cr Diffusion Measurements . . . . .	111
B. Data for Radiotracer Experiments . . . . .	118
APPENDICES REFERENCES . . . . .	126
VITA . . . . .	128

LIST OF TABLES

TABLE	PAGE
I. Equilibrium Concentrations of Cr Fluorides for the Reaction of Pure Cr with UF <sub>4</sub> . . . . .	9
II. Compositions of Experimental Alloys Used for Corrosion Studies . . . . .	15
III. Compositions of INOR-8 Thermal Convection Loops	16
IV. Composition of Fluoride Mixture Used To Evaluate Experimental Ni-Mo Alloys . . . . .	21
V. Corrosion-Product Concentrations of Salts Tested with Ni-Mo-Cr Alloys . . . . .	36
VI. Corrosion-Product Concentrations of Salts Tested with Ni-Mo Alloys Containing Cr in Combination with Other Alloying Elements . .	41
VII. Corrosion-Product Concentrations of Salts Tested with Ni-Mo-Al Alloys . . . . .	48
VIII. Corrosion-Product Concentrations of Salts Tested with Ni-Mo Alloys Containing Al in Combination with Other Alloying Elements . .	50
IX. Corrosion-Product Concentrations of Salts Tested with Ni-Mo Alloys Containing Ti . . . .	54
X. Corrosion-Product Concentrations of Salts Tested with Ni-Mo Alloys Containing V and Fe .	57
XI. Corrosion-Product Concentrations of Salts	

TABLE	PAGE
Tested with Ni-Mo-Nb Alloys . . . . .	61
XII. Corrosion-Product Concentrations of Salts	
Tested with Ni-Mo Alloys Containing Nb in	
Combination with Other Alloying Elements . . .	62
XIII. Corrosion-Product Concentrations of Salts	
Tested with Ni-Mo Alloys Containing W . . . .	65
XIV. Relative Thermodynamic Stabilities of Fluoride	
Compounds Formed by Elements Employed as	
Alloying Additions . . . . . . . . . . .	68
XV. Properties of INOR-8 Specimens and Salt Mix-	
tures Used for Radiotracer Loop Experiments .	119
XVI. Total Specimen Radioactivities and Corresponding	
Cr Diffusivities Measured in INOR-8 Loop 1248	
after 500-hr Exposure to Salt . . . . .	120
XVII. Total Specimen Radioactivities and Corresponding	
Cr Diffusivities Measured in INOR-8 Loop 1249	121
XVIII. Sample Calculations of Cr Diffusivities Based	
on Concentration Gradient of Cr-51 in	
Specimens from Loop 1248 . . . . . . . . .	122
XIX. Sample Calculations of Cr Diffusivities Based	
on Concentration Gradient of Cr-51 in	
Specimens from Loop 1249 . . . . . . . . .	123
XX. Cr Diffusivities Measured in INOR-8 Loop 1248	
Based on Cr-51 Concentration Profile . . . . .	124

## TABLE

## PAGE

XXI. Cr Diffusivities Measured in INOR-8 Loop 1249

Based on Cr-51 Concentration Profile . . . . . 125

## LIST OF FIGURES

FIGURE	PAGE
1. Schematic Diagram of Thermal Convection Loop Used for Evaluations of Experimental Ni-Mo Alloys . . .	18
2. Photograph of Assembled Thermal Convection Loops and Test Stands . . . . .	23
3. Design of Thermal Convection Loops 1248 and 1249 Used for Radiotracer Experiments . . . . .	29
4. Specimen Locations and Temperatures as a Function of Position Along Loop 1248 . . . . .	31
5. Concentration of Cr Ions in Salt 107 as a Function of Cr Content in Ni-Mo-Cr Alloys . . . . .	37
6. Concentration of Cr Ions in Salt 107 as a Function of Cr Content in Ni-Mo Alloys Containing Multiple Alloy Additions . . . . .	42
7. Appearance of Hot-Leg Surface of Ternary Ni-Mo Alloy Containing 5.55 Atomic Per Cent Cr Follow- ing Exposure to Salt 107 . . . . .	45
8. Hot-Leg Sections of Ni-Mo-Cr Thermal Convection Loops Following 500-hr Exposure to Salt 107 . . .	46
9. Depths of Corrosion Observed for Ni-Mo Alloys with Multiple Alloy Additions Following Exposure to Salt 107 . . . . .	47
10. Hot-Leg Surface of Ternary Ni-Mo Alloy Containing 4.27 Atomic Per Cent Al after 1000-hr Exposure	

FIGURE	PAGE
to Salt 107 . . . . .	52
11. Hot-Leg Surface of Ternary Ni-Mo Alloy Containing 2.47 Atomic Per Cent Ti after 1000-hr Exposure to Salt 107 . . . . .	55
12. Attack at Hot-Leg Surface of Ternary Ni-Mo Alloy Containing 5.11 Atomic Per Cent V . . . . .	59
13. Appearance of Voids in Ni-Mo Alloy Containing 3.62 Atomic Per Cent Nb after 1000-hr Exposure to Salt 107 . . . . .	63
14. Hot-Leg Surface of Ni-Mo Alloy Containing 1.44 Atomic Per Cent W after 500-hr Exposure to Salt 107 . . . . .	66
15. Comparison of Corrosion-Product Concentrations Formed in Salt 107 by Various Alloying Additions as a Function of Alloy Content . . . . .	70
16. Relation between Temperature and Cr-51 Diffusion Coefficients Determined in INOR-8 Loop 1248 . . .	76
17. Per Cent of Cr Tracer Remaining as a Function of Depth of Removal from Surface of Specimen No. 15, Loop 1248 . . . . .	78
18. Comparison of Diffusion Coefficients for Cr in Ni-Base Alloys . . . . .	80
19. Comparison of Surfaces of INOR-8 Loop 1248 before and after Exposure to NaF-ZrF <sub>4</sub> Salt Containing	

FIGURE	PAGE
$\text{Cr}^{51}\text{F}_2$	81
20. Relation between Temperature and Cr-51 Diffusion Coefficients Determined in INOR-8 Loop 1249 . . .	85
21. Per Cent of Cr Tracer Remaining as a Function of Depth of Removal from Surface of Specimen No. 15, Loop 1249 . . . . .	86
22. Comparison of Predicted and Actual Cr Concentration Profiles in Specimen No. 15, Loop 1249 . . . .	89
23. Appearance of Cold- and Hot-Leg Sections of Loop 1249 after Exposure to $\text{NaF-ZrF}_4$ Salt Containing $\text{FeF}_2$ . . . . .	92
24. Calculated Corrosion Rate and Cumulative Attack for 800°C Section of INOR-8 Loop Containing Pre-Equilibrated $\text{NaF-ZrF}_4-\text{UF}_4$ (50-46-4 mole per cent) Salt . . . . .	101

## CHAPTER I

### INTRODUCTION

Molten fluorides of U, Th, or Pu, in combination with other fluoride compounds, have wide applicability as fuels for the production of nuclear power.<sup>1\*</sup> Because of their high boiling points, these mixtures can be contained at low pressures even at extremely high operating temperatures. Their chemical and physical properties impart additional advantages, such as excellent stability under irradiation and large solubility ranges for both U and Th. These factors have prompted design studies of molten fluoride fuel systems in conjunction with Th-U thermal breeders, U-Pu converters, and U burners. A high-temperature nuclear reactor, designated the Aircraft Reactor Experiment (ARE), was successfully operated to demonstrate the feasibility of the latter concept.<sup>2</sup>

The development of reactors which incorporate a circulating fluoride salt is predicated on the availability of a construction material which will contain the salt over long time periods and also afford useful structural properties. Paramount among the materials requirements which must be fulfilled are the following: resistance to corrosion by the

---

\*Superscript figures designate citations documented in the List of References, pages 106-7, 125.

fluoride fuel, particularly in the presence of a neutron flux; resistance to air oxidation; and satisfactory high-temperature mechanical properties. It is also required that the container material be easily formed and welded into relatively complicated shapes and that it be metallurgically stable over a wide temperature range.

In order to provide a material for initial reactor studies, several commercially-available high-temperature alloy systems were evaluated with respect to the above requirements by the Metallurgy Division at Oak Ridge National Laboratory. As a result of these studies, Inconel, a Ni-base alloy containing 15 Cr, 7 Fe\*, was found to afford the best compromise of desired properties and was utilized for the construction of the ARE.<sup>3</sup> Extensive corrosion tests, as well as post-test examinations of the ARE, confirmed the suitability of Inconel as a container material for relatively short-term fluoride salt exposures. Corrosion rates encountered with this alloy at temperatures above 700°C, however, were excessive for long-term use with most fluoride fuel systems.

Utilizing experience gained in corrosion testing of commercial alloys, an alloy development program was initiated at ORNL to provide an advanced container material for

---

\*Compositions refer to per cent by weight, except where otherwise noted.

fluoride fuel reactor systems. The alloy system used as the basis for this program was composed of Ni with a primary strengthening addition of 15-20 per cent Mo. This composition afforded exceptional resistance to fluoride attack but lacked sufficient mechanical strength and oxidation resistance at desired operating temperatures. To augment these latter properties, additions of various solid-solution alloying agents were evaluated, among them Cr, Al, Ti, Nb, Fe, V, and W. An optimum alloy composition was selected on the basis of parallel investigations of the mechanical and corrosion properties which were imparted by each of these additions. The composition best suited to reactor use was determined to be within the range 15-17 Mo, 6-8 Cr, 4-6 Fe, 0.04-0.08 C, balance Ni. Subsequent studies of the alloy, designated INOR-8, showed it to be extremely well suited for applications demanding long-term compatibility with fluoride salts in the temperature range 650°-800°C.

The present research was concerned with the corrosion effects resulting from additions of alloying elements to the Ni-Mo system and an analysis of the diffusion rates of Cr in the INOR-8 alloy under representative service conditions.

## CHAPTER II

### OBJECTIVES

The general objective of the present research was the evaluation of the corrosion behavior of Ni-Mo alloy systems in fluoride fuel mixtures. Studies were carried out in three chronological phases:

1. An analysis of the effects of additions of Cr, Fe, Nb, V, W, Al, and Ti on the corrosion properties of Ni-base alloys containing 15-20 per cent Mo, which culminated in the selection of an optimum alloy composition.
2. Application of radiotracer techniques to the study of the diffusion rates of Cr in the selected alloy.
3. Application of the diffusion rate data to the prediction of corrosion rates for the selected alloy.

## CHAPTER III

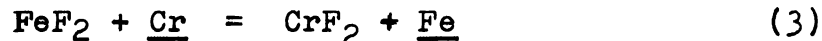
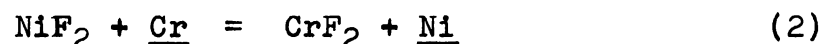
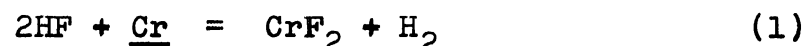
### REVIEW OF RELATED WORK

#### I. CORROSION BY FLUORIDE MIXTURES

##### Corrosion Reactions

The corrosion of Ni-base alloys, containing Fe and Cr, by fluoride fuel mixtures has been found to result from a combination of the following types of oxidation reactions:<sup>4</sup>

1) Reactions\* involving impurities in the salt

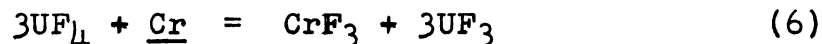
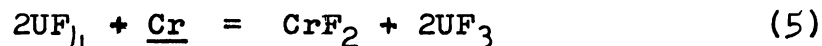


2) Reactions involving impurities in or on the metal, for example



followed by reaction (2)

3) Reactions involving components in the salt



The extent of the first four of these reactions, which proceed strongly to the right and to completion rapidly, can be reduced by maintaining low impurity concentrations in the

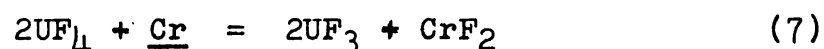
---

\*Solid-solution alloying elements are underlined.

salt and on the surface of the metal. Reactions (5) and (6), on the other hand, are ever-present in fluoride systems which derive their usefulness through the containment of  $\text{UF}_4$  and have been found to play a major role in the corrosion of Cr-containing alloys. While the role of Cr in this connection has been investigated extensively,<sup>5</sup> considerably less information is available regarding the thermodynamic properties of the reaction for the other alloying elements which were of interest in the present study.

#### Reduction of $\text{UF}_4$ by Cr

The reaction of  $\text{UF}_4$  with Cr was found to be strongly influenced by the reaction medium employed.<sup>6</sup> In melts composed principally of  $\text{NaF-ZrF}_4$  or  $\text{NaF-BeF}_2$ , the reaction produced only divalent Cr, i.e.:



The equilibrium constant for this reaction is given by

$$K_a = \frac{(a_{\text{CrF}_2})(a_{\text{UF}_3})^2}{(a_{\text{UF}_4})^2(a_{\underline{\text{Cr}}})} \quad (8)$$

where  $a$  represents thermodynamic activity. Because of the relatively small concentrations of  $\text{CrF}_2$  and  $\text{UF}_3$  which are attained in the salt solutions at equilibrium, the activities of each of these components can be closely approximated by their mole fractions, in accordance with Henry's law. Thus, for a salt system of fixed  $\text{UF}_4$  concentration, assuming the

reference states for salt components to be the infinitely dilute solution,

$$K_a = \frac{(N_{CrF_2})(N_{UF_3}^2)}{(a_{UF_4}^2)(a_{Cr})} \quad (9)$$

and

$$N_{CrF_2} \cdot N_{UF_3}^2 = K'_1 a_{Cr} \quad (10)$$

where

$$K'_1 = K_a a_{UF_4}^2$$

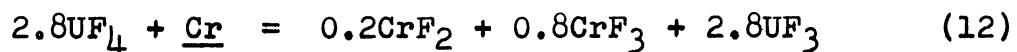
It will be noted from equation 6 that in those systems for which the only active components present initially are Cr in the alloy and  $UF_4$  in the salt,  $N_{CrF_2} = \frac{1}{2}N_{UF_3}$ . Accordingly, for such systems equation 10 reduces to

$$N_{CrF_2} = K'_1 a_{Cr}^{1/3} \quad (11)$$

where

$$K'_1 = \left(\frac{K'_1}{4}\right)^{1/3}$$

In the case of NaF-KF-LiF- $UF_4$  mixtures, the reaction between Cr and  $UF_4$  produced both divalent and trivalent Cr. At equilibrium, approximately 80 per cent of the total Cr ions in the mixtures was observed to be trivalent, so that the net reaction could be written as



for which

$$K_a = \frac{(N_{CrF_2})^{0.2} (N_{CrF_3})^{0.8} (N_{UF_3})^{2.8}}{(A_{UF_4})^{2.8} (A_{Cr})} \quad (13)$$

For a system initially containing no  $UF_3$ ,  $CrF_2$ , or  $CrF_3$ , it follows that  $N_{CrF_2} = 1/4 N_{CrF_3} = 1/14 N_{UF_3}$ . In such systems, for constant  $UF_4$  concentrations, equation 12 reduces to

$$(N_{CrF_2} + N_{CrF_3}) = K_2 A_{Cr}^{5/19} \quad (14)$$

where

$$K_2 = 5 \left( \frac{K_a}{4} \right)^{4/19} \left( \frac{A_{UF_4}}{14} \right)^{14/19}$$

The constants  $K_1$  and  $K_2$  have been experimentally determined for mixtures of  $NaF-ZrF_4-UF_4$  (50-46-4 mole per cent) and  $LiF-KF-NaF-UF_4$  (11.2-41.0-45.3-2.5 mole per cent), respectively, by equilibrating the mixtures with pure Cr ( $A_{Cr} = 1$ ) at  $600^{\circ}C$  and  $800^{\circ}C$ .<sup>7</sup> Under these conditions, the constants are equivalent in value to the mole fraction of Cr ions in the salt at equilibrium. Some representative values are listed in Table I. It is evident that the temperature dependence in the case of the  $ZrF_4$ -bearing mixture is smaller than that for the alkali-metal fluoride system.

Because of the temperature dependence of the  $Cr-UF_4$  reaction, chemical equilibrium between these two components is precluded in polythermal systems, i.e., systems of uniform

TABLE I

EQUILIBRIUM CONCENTRATIONS OF Cr FLUORIDES  
FOR THE REACTION OF PURE Cr WITH  $\text{UF}_4$   
(Data of J. D. Redman)<sup>7</sup>

Equilibration Temperature (°C)	Concentrations of Cr ions in <u>NaF-ZrF<sub>4</sub>-UF<sub>4</sub></u> (50-46-4 mole %)		Concentrations of Cr ions in <u>NaF-LiF-KF-U<sub>4</sub></u> (11.2-41.0-45.3-2.5 mole %)	
	<u>ppm</u>	<u>mole fraction (K<sub>1</sub>)</u>	<u>ppm</u>	<u>mole fraction (K<sub>2</sub>)</u>
600	2200	$4.7 \times 10^{-3}$	1100	$1.0 \times 10^{-3}$
800	2500	$5.4 \times 10^{-3}$	2600	$2.4 \times 10^{-3}$

alloy composition in which the circulating salt continually experiences a temperature change. In such systems Cr tends to be continually removed from hotter portions and deposited in cooler portions. A theory relating the rate of this movement to the operating parameters of the container system was formulated by Evans.<sup>8</sup> This theory postulated that mass transport rates were controlled by the diffusion rate of Cr in the container material and that Cr concentrations at the container surface were at all times in equilibrium with the  $\text{UF}_4$ ,  $\text{UF}_3$ , and  $(\text{CrF}_2, \text{CrF}_3)$  salt components. Computations of mass transport rates were then obtained through solutions of diffusion equations under surface conditions predicted by thermodynamic data for the Cr- $\text{UF}_4$  reaction.

## II. CORROSION OF Ni-Mo ALLOYS

Because of the oxidation of Cr by fuel-bearing fluoride salts, alloys employing large percentages of this element were not satisfactory as container materials except at temperatures where diffusion rates in the alloys were relatively low. Accordingly, evaluations were made of several commercial alloys in which Cr was not employed as a major alloying addition. Based on these tests, alloys of Ni and Mo appeared to offer the most promising container system for achieving relatively high reactor operating temperatures. Unfortunately, commercially-available Ni-Mo alloys which exhibited excellent

corrosion properties were not well suited to contemplated reactor systems because of three adverse characteristics:

1) poor fabricability; 2) a tendency to age-harden and embrittle at service temperatures between 650° and 815°C;<sup>9</sup> and 3) poor resistance to oxidation by air at elevated temperatures. The scale formed on exposure of these alloys to high-temperature air was of the type NiMoO<sub>4</sub>, which upon thermal cycling between 760° and 350°C underwent a phase transformation and spalled as a consequence of a resultant volume change.<sup>10</sup>

By means of an alloy development program, however, it was considered plausible to eliminate the undesirable features of the commercial materials while retaining their inherent corrosion resistance. The initial objective of this program was to provide an alloy which did not embrittle under the thermal treatments imposed by reactor operation. By experimenting with various compositions of binary Ni-Mo alloys, it was determined that lowering the Mo concentration to a level of 15-17 per cent served to avoid detrimental age-hardening effects in the alloy system.<sup>11</sup> Although such an alloy system was ideal from the standpoint of corrosion resistance, it was necessary to augment the oxidation and strength characteristics of the system through additional solid-solution alloying agents. The corrosion effects which resulted from these additions and the corrosion properties of the finalized alloy

modification, INOR-8, were the subjects of the present study.

## CHAPTER IV

### MATERIALS AND PROCEDURES

The test techniques described in this section were applied both to corrosion studies of experimental Ni-Mo alloys and to subsequent studies of INOR-8. In the latter studies the incorporation of a radioactive tracer necessitated certain modifications in the operating procedures and test analysis. These modifications are discussed in the second part of this section.

#### I. EFFECTS OF ALLOYING ADDITIONS

##### Test Materials

The Ni-Mo alloy compositions used for studies of alloying effects on corrosion behavior were supplied by the Metallurgy Division of ORNL and, under subcontract agreements, by Battelle Memorial Institute and Superior Tube Company. Alloys furnished by ORNL were induction-melted under vacuum, while those furnished by subcontractors were induction-melted in air using a protective slag. Each alloy heat, which ranged in weight from 12 to 100 lbs, was either forged or extruded into a 3-in. diameter tube blank and was subsequently drawn into seamless tubing, 1/2-in. OD and 0.035-in. wall thickness, by the Superior Tube Company. The cold-drawn

tubing was annealed at 1121°C. A listing of the experimental alloy compositions is given in Table II.

Corrosion studies of INOR-8 were conducted with commercially-produced seamless tubing of the compositions shown in Table III. This material had also been given a 1121°C annealing treatment following the final cold reduction.

#### Test Equipment

The test method used for evaluating the corrosion properties of the experimental alloys was selected on the basis of the following considerations:

1) The method necessarily had to be tailored to the use of relatively small quantities of material, since it was practical to produce only small heats of the vast number of alloys desired for study.

2) Tubing was considered to be a highly desirable form in which to test the material, since production of the material in this form was carried out as an adjunct to evaluating the fabricability of each alloy.

3) Previous demonstrations of the effects of temperature gradient in the salt and the salt flow rate on the corrosion behavior of container materials in fluorides made it mandatory that corrosion tests be conducted under dynamic conditions, i.e., conditions which provided for the continuous flow of salt through a temperature gradient.

TABLE II  
COMPOSITIONS OF EXPERIMENTAL ALLOYS USED FOR CORROSION STUDIES

Heat No*	Composition (weight %)								Composition (atomic %)								
	Ni	Mo	Cr	Fe	Ti	Al	Nb	W	V	Ni	Mo	Cr	Fe	Ti	Al	Nb	W
<b>Series I:</b>																	
OR 30-1	80.12	16.93	2.83							85.50	11.10	3.41					
OR 30-2	78.55	16.65	4.62							83.60	10.80	5.55					
OR 30-4	73.65	16.37	9.21							78.30	10.60	11.04					
OR 30-6	78.50	15.11	6.40							82.70	9.72	7.60					
OR 37A-1	77.0	20.39	2.62							83.30	13.50	3.20					
OR 43A-3	73.30	20.34	6.34							78.90	13.40	7.71					
<b>Series II:</b>																	
OR 30-7	82.10	15.93							1.88								
OR 30-8	80.30	17.80							1.89								
OR 30-9	81.10	16.8								2.09							
OR 30-10	81.10	16.60								2.23							
OR 30-11	79.80	16.53									3.68						
OR 30-12	80.00	16.80									3.22						
OR 30-19	79.00	16.90									4.10						
OR 30-20	79.20	16.60									4.18						
OR 30-21	78.90	16.40									4.71						
S T23012	82.00	17.42									0.53						
OR 1491	86.58	11.23									2.19						
<b>Series III:</b>																	
OR 30-13	79.93	17.56							1.56	0.95							
OR 30-14	79.53	16.50							1.52	2.45							
OR 30-16	77.74	16.00	3.65						1.49	1.12							
OR 30-22	77.65	15.90	5.69						1.16	0.60							
OR 30-33	74.07	15.15	5.01	5.07					0.70								
B2897	76.13	20.50							1.25	1.32							
B2898	76.30	20.50							2.44	1.31							
B3276	69.19	21.10	7.58							2.16							
B3277	66.95	21.60	7.82							1.31	2.32						
S T23011	71.50	15.06	3.84							0.53	4.17	4.90					
S T23013	74.42	15.20								0.58	4.57	5.23					
S T23014	80.86	16.70							2.10	0.57							

\*OR denotes heats furnished by the ORNL Metallurgy Division.

S T denotes heats furnished by Superior Tube Company.

B denotes heats furnished by Battelle Memorial Institute.

TABLE III  
COMPOSITIONS OF INOR-8 THERMAL CONVECTION LOOPS

Loop No.	Composition (weight %)					Composition (atomic %)				
	Ni	Mo	Cr	Fe	C	Ni	Mo	Cr	Fe	C
1248	69.8	16.5	6.90	5.10	0.073	75.0	10.8	8.4	5.7	-
1249	72.7	15.0	7.41	4.72	0.078	76.5	9.6	8.8	5.1	-

The thermal convection loop, which had been used extensively for Inconel corrosion studies and had been developed into an extremely straightforward and reliable test device, was judged to be the best form of experimental device for meeting these requirements. This device consists of a closed loop of tubing, bent to resemble the outline of a harp, two legs of which are heated and two of which are exposed to the cooling effects of ambient air. A flow velocity is thus generated by the difference in density of the salt in the hot and cold portions of the loop.

A schematic diagram illustrating the configuration and dimensions of the loop design employed is presented in Figure 1. All loops were comprised of seamless tubing having an outside diameter of 0.500 in. and a wall thickness of 0.035 in. The tubing was assembled by the Heliarc welding technique using an inert gas backing.

The loops were heated by six sets of Hevi-Duty tubular furnace heating elements as shown in Figure 1. Each set of elements was 6 in. in length and 1-1/4 in. in inside diameter. The heaters were centered on the tubing and were separated by means of ceramic spacers inserted in the ends. The heaters were connected in two parallel electrical circuits, and the power was supplied from saturable core reactors.

While filling the loop with salt solution, it was necessary to apply heat to both the cold-leg and hot-leg

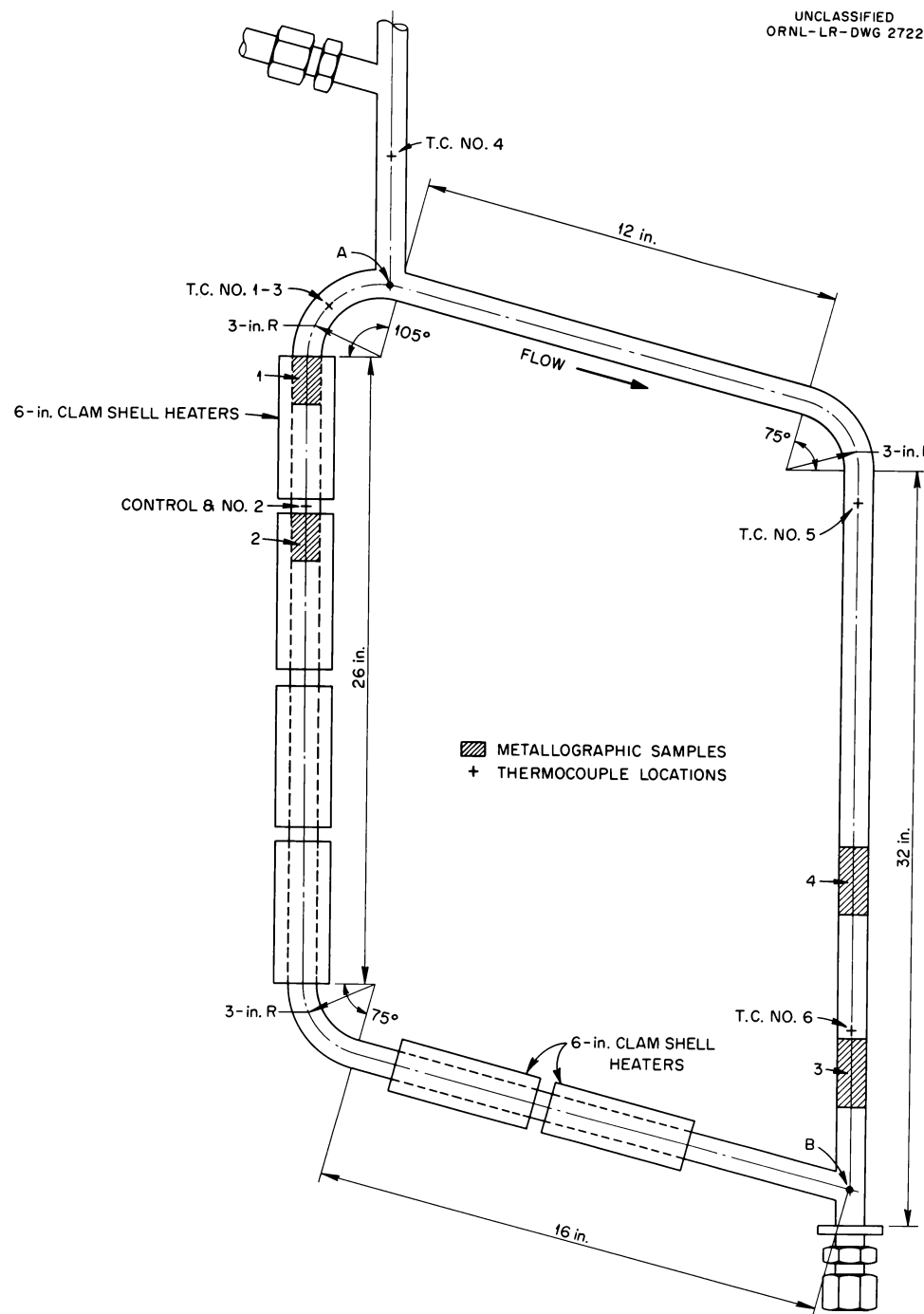
UNCLASSIFIED  
ORNL-LR-DWG 27228 R

Figure 1. Schematic diagram of thermal convection loop used for evaluations of experimental Ni-Mo alloys. The locations of thermocouples and test samples are shown.

sections. Auxiliary heating for this purpose was provided by passage of electricity directly through the tube wall. Once the loop had been filled, the auxiliary heat source was turned off and the heating elements were turned on. Insulation was applied to both hot- and cold-leg sections of the loop during filling. When the loop was filled, as determined by an electrical shorting probe near the top of the loop, insulation was removed from the cold leg to whatever amount was required to establish a pre-determined temperature gradient.

Loop temperatures were measured with Chromel-Alumel thermocouples located as shown in Figure 1. The thermocouple junctions, in the form of small beads, were welded to the outside tube wall with a condenser discharge welder and covered by a layer of quartz tape, which in turn was covered with stainless steel shim stock.

The power input to the loops was controlled by Leeds and Northrup Micromax proportional controllers utilizing thermocouples located between the two heaters in the top portion of the loop.

All tests were operated so as to achieve a maximum mixed-mean salt temperature of 815°C and a minimum salt temperature of 650°C. The maximum salt-metal interface temperature, which was attained near the top of the vertical heated section, exceeded the maximum bulk salt temperature by

approximately 95°C.\* The salt flow rate under these temperature conditions was established from heat balance calculations to be in the range of 5 to 7 ft/min.

#### Salt Preparation

The compositions of the fuel mixture used in the experimental Ni-Mo alloy studies are shown in Table IV. The selection of the LiF-KF-NaF-UF<sub>4</sub> composition (Salt 107) was made on the basis that the oxidation of container constituents by a given concentration of UF<sub>4</sub> tended to be greater for this mixture than for other mixtures of practical importance. Thus, achievement of satisfactory compatibility with this mixture in effect provided a container material of ultimate versatility with respect to all fuel mixtures.

The fluoride mixtures were prepared from reagent-grade materials and were purified by the Fluoride Processing Group of the Reactor Chemistry Division. In general, the procedure for purification was as follows: 1) the dry ingredients, except for UF<sub>4</sub>, were mixed, evacuated several times for moisture removal, and then melted under an atmosphere of He;

---

\*Measurements of the maximum inside wall temperature could not practically be made in each loop test; however, values of this temperature were recorded by means of heat balance calculations and imbedded thermocouples using a specially-instrumented test loop which exactly simulated the geometry and temperature profile used in the corrosion experiments.

TABLE IV

COMPOSITION OF FLUORIDE MIXTURE USED TO  
EVALUATE EXPERIMENTAL Ni-Mo ALLOYSSalt No. 107  
Liquidus Temperature, 490°C

<u>Component</u>	<u>Mole %</u>	<u>Weight %</u>
NaF	11.2	9.79
LiF	45.3	24.4
KF	41.0	49.4
UF <sub>4</sub>	2.5	16.3

2) the molten mixture was held at 815°C and treated with H<sub>2</sub> for 4 hours to purge HF from the mixture; 3) the mixture was cooled to 205°C under a He atmosphere and UF<sub>4</sub> was admitted. Upon the addition of the UF<sub>4</sub>, the mixture was remelted, heated to 815°C, and then treated again with H<sub>2</sub> to purge the excess HF.

All mixtures were prepared in 300-lb quantities and apportioned into 50-lb containers, after which samples were submitted for analysis of Ni, Fe, and Cr. It was required that each of these elements be present in amounts less than 500 ppm as determined from individual batch analyses. A second before-test analysis of each salt mixture was obtained from a sample of the salt taken as it was being admitted to the test loop.

#### Operating Procedures

Each loop was thoroughly degreased with CH<sub>3</sub>•CO•CH<sub>3</sub> and checked for leaks using a He mass spectrometer which, with the inside of the loop at a pressure of <5μ Hg, measured the leak rate of He into the loop. After thermocouples and heaters were assembled and insulation was applied, the loop was placed in a test stand. A photograph of the test assembly is shown in Figure 2.

Ni or Inconel tubing, 1/4-in. OD, was used to connect the salt-charging-pot to the loop. All connections were made

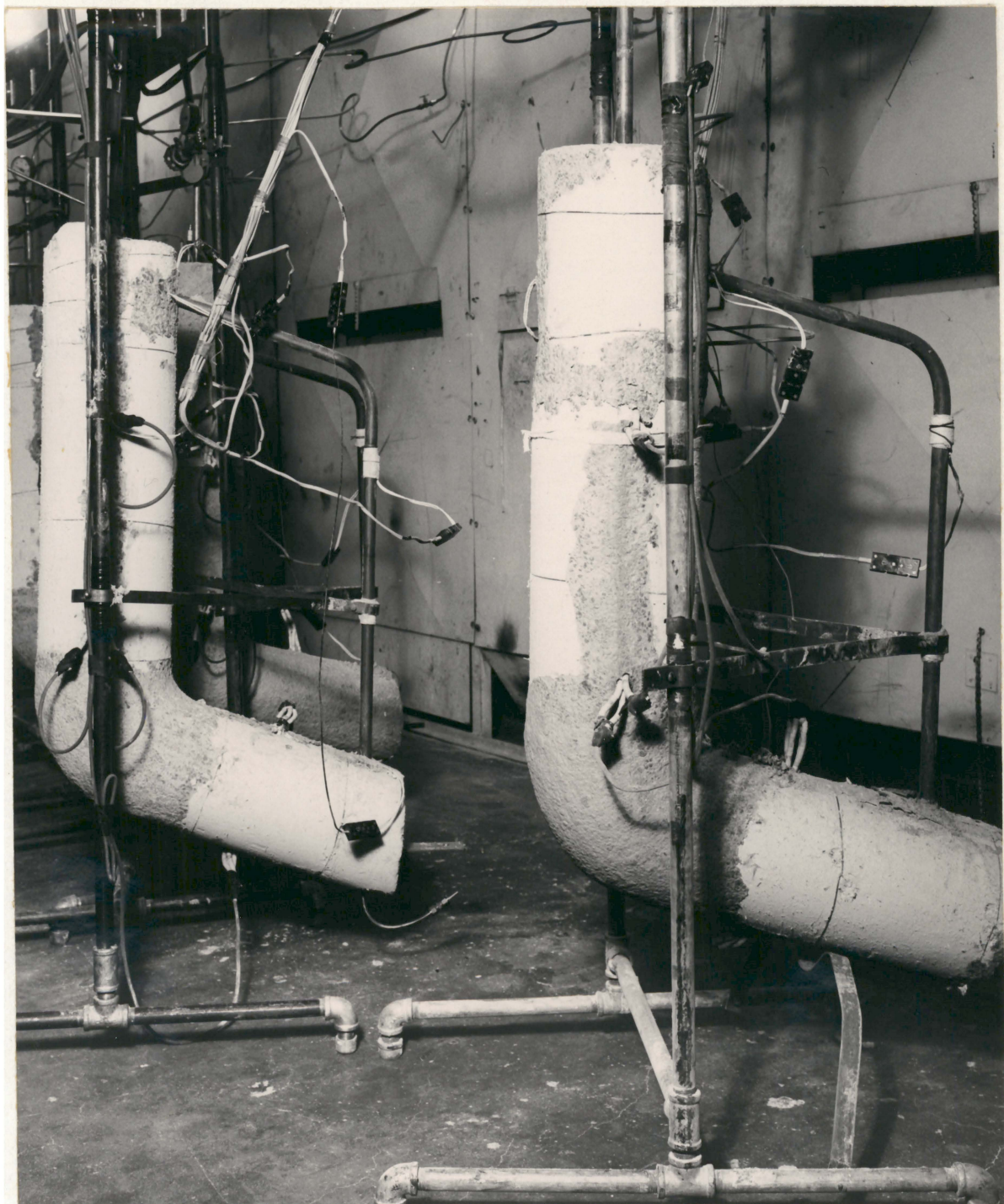


Figure 2. Photograph of assembled thermal convection loops and test stands.

with Swagelok fittings. Both the loop and the charging-pot were heated to 650°C under a dynamic vacuum of  $< 50 \mu$  Hg. He pressure was then applied to the charge-pot in order to force the salt mixture from the pot to the loop. After filling, salt was allowed to stand in the loop at 650°C for approximately 2 hours, so that oxides and other impurities would be dissolved from the container surface into the salt mixture. This mixture was then removed, and a fresh salt mixture was admitted from the fluoride-charging-pot still connected to the loop. Insulation was then removed from the cold-leg and the hot-leg temperature was increased to 815°C. A He cover gas under slight positive pressure (approximately 5 psig) was maintained over the salt mixture during all periods of testing.

At the end of a given test period, power to the loop was cut off and insulation was stripped from the loop so as to freeze the salt mixture as rapidly as possible.

#### Test Examination

After cooling, each loop was sectioned with a tubing cutter into approximately 6-in. lengths. Five 2-in. sections were then removed from the loop positions indicated in Figure 1 for metallographic examination. Two of the remaining 6-in. sections, one from the hottest section of the loop (specimen H) and one from the coldest section (specimen C), were

obtained for salt chemistry studies, and the remaining loop segments were held in storage until all examinations of the loop were completed.

Salt removal was accomplished by heating each section in a small tube furnace at 600°C in He. The salt was collected in a graphite crucible located below the furnace windings. The five 2-in. sections of tubing were examined metallographically and the salt samples were submitted individually for petrographic and chemical analyses. If layers of corrosion products were discovered on the tube wall, samples of the tubing and salt contained in that section were also submitted for X-ray diffraction examination.

Metallographic examination. Both longitudinal and transverse sections of each specimen were examined metallographically. The surfaces of all cold-leg specimens were Ni-plated before sectioning to retain any corrosion products. Specimens were polished mechanically and were etched using a solution of 90 parts HCl, 5 parts HNO<sub>3</sub>, 5 parts H<sub>2</sub>SO<sub>4</sub>, and 1 part HF. They were then examined under bright-field illumination for evidence of corrosive attack.

Chemical analyses. Salt specimens were finely ground, and weighed portions were dissolved in HCl-HNO<sub>3</sub>-H<sub>2</sub>SO<sub>4</sub>. The resultant solution was exposed to SO<sub>3</sub> fumes to drive off all acid components but H<sub>2</sub>SO<sub>4</sub> and diluted so as to contain

approximately 5 per cent acid by volume. Aliquot portions were then submitted for quantitative analyses of all elemental constituents which had comprised the alloy to which the salt had been exposed. All chemical analyses were performed by the Reactor Project Analytical Laboratory.

## II. RADIOTRACER TECHNIQUES

The radiotracer Cr-51 was applied to the determination of diffusivities of Cr in INOR-8 and to an evaluation of corrosion mechanisms which purportedly govern Cr mass transport in this alloy. The procedure employed for measuring Cr diffusion rates in INOR-8 was based on a tracer method which had been applied by Evans<sup>12</sup> to determinations of Cr diffusivities in Inconel. This method, which is outlined in Appendix A, establishes a known concentration of Cr-51 at the surface of the alloy in contact with a fluoride salt mixture containing radioactive CrF<sub>2</sub>. As discussed in Appendix A, the thermal convection loop provides an optimum test vehicle for conducting diffusion experiments of this type, since in a single loop experiment diffusivities may be determined simultaneously for a wide range of temperatures.

A single INOR-8 thermal convection loop (No. 1248) was operated with a CrF<sub>2</sub>-containing salt to determine diffusion rates of Cr in this alloy between 650° and 910°C. The salt used was NaF-ZrF<sub>4</sub> (53-47 mole per cent) and contained 1800

ppm of CrF<sub>2</sub>, a known quantity of which was radioactive.

#### Chromium Tracer

The isotope Cr-51 emits a gamma ray of energy 0.32 Mev and has a half-life of approximately 27 days. As the duration of the diffusion experiment was not expected to exceed more than twice this half-life, this isotope appeared well suited to the experiment. Accordingly, a salt composed of extremely pure CrF<sub>2</sub>, prepared by the ORNL Reactor Chemistry Division,<sup>13</sup> was irradiated in the X-10 graphite reactor to convert a small percentage of the Cr-50 nuclides in this compound to Cr-51. The radioactivity induced was sufficiently low so that, when dissolved in the carrier salt, the resultant mixture could be handled without shielding.

#### Molten Fluoride Solvent

The molten fluoride mixtures were prepared from reagent-grade materials and were purified in a closed system of Ni at 800°C by alternate flushing with anhydrous HF and H<sub>2</sub>. The apparatus and procedure were identical with those described for salts used for corrosion testing of Ni-Mo alloys.

#### Counting Techniques

A well-type scintillation counter was employed for all

count rate determinations of gamma rays emitted by Cr-51. Undesirable geometry and shielding effects which might have introduced counting errors were eliminated or minimized as described elsewhere.<sup>14</sup>

#### Test Apparatus

A schematic diagram of the loop in which the tracer-containing salt was circulated is shown in Figure 3. This loop differed from the standard convection loop design (Figure 1) only in that it incorporated a 3-in. diameter sampling pot at the top of the hot-leg section. Additional thermocouples were also used in conjunction with the tracer loop to provide temperature readings at every point in the loop from which specimens were taken for diffusion rate studies. The sampling pot provided additional ports for tracer additions and salt-sample withdrawals. It also served to increase the loop volume and permit the removal of salt samples without noticeably changing the salt level in the loop.

#### Operating Procedure

The construction and operation of the tracer loop experiment followed the same general procedures as those described for standard convection-loop experiments, including the preliminary salt exposure to remove any surface

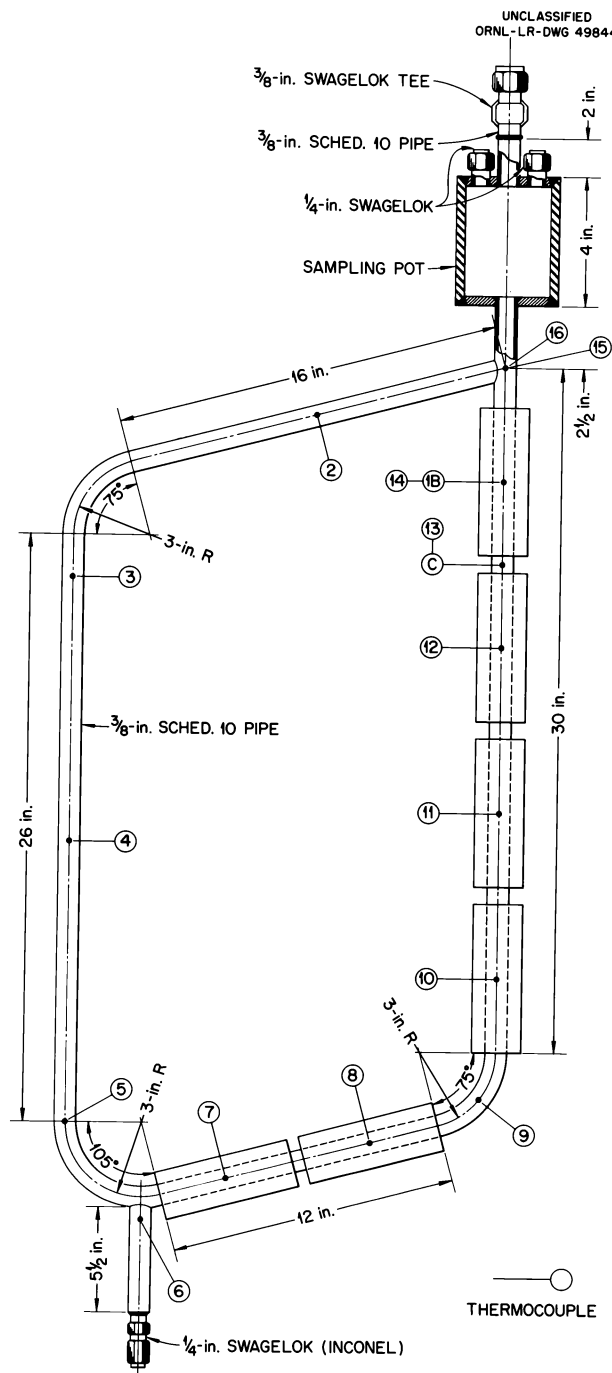


Figure 3. Design of thermal convection Loops 1248 and 1249 used for radiotracer experiments. Thermocouple locations and designations are shown by circled numbers and letters.

contaminants.

Once the tracer-containing salt had been admitted to the loop, the loop was quickly brought to the desired operating temperatures, which were then maintained within a range of  $\pm 5^{\circ}\text{C}$  throughout the experiment. The loop wall-salt interface temperatures which were established throughout the loop are shown in Figure 4. All temperatures except those at positions directly under heaters were determined directly from thermocouple readings. Those under the heaters were determined from heat balance calculations and, in the case of the maximum interface temperature, by the use of thermocouples imbedded in the loop wall.

Samples of salt weighing approximately 2 gm were withdrawn from the sampling pot loop at one-day intervals for a period of 5 days and at weekly intervals thereafter. Although it was planned to add radioactive  $\text{CrF}_2$  to the salt during the course of operation as required to maintain a constant surface Cr-51 concentration, the overall loss of tracer indicated by the salt samples was insufficient to warrant replacement.

After 500 hours at temperature, all sections of the loop were quickly cooled to  $600^{\circ}\text{C}$ ; the salt was then drained from the loop, all power to the loop was cut, and the insulation was removed to allow the loop to cool rapidly to room temperature.

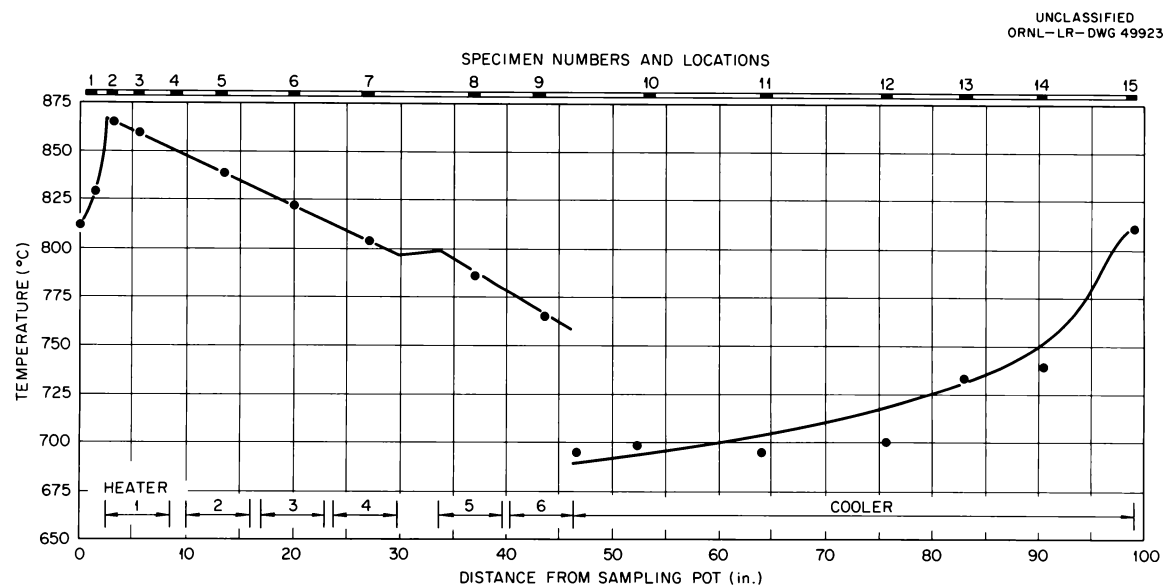


Figure 4. Specimen locations and temperatures as a function of position along Loop 1248. Temperatures of cold-leg specimens (Nos. 10 through 15) were obtained from thermocouples 2 through 6 shown in Figure 3. Temperatures of specimens 1 through 9, which were located under or close to heaters, were obtained from heat balance calculations, represented by the solid black line.

Test Analysis

Following termination of a given loop run, fifteen 1-1/2-in. sections were removed from various positions along the loop, as indicated in Figure 3. Each of these samples was accurately machined to an overall length of 1-3/16 in., and the ends were undercut to leave a 1-in. section of undisturbed tubing. The samples were then cleaned in dilute  $\text{NH}_4\text{HC}_2\text{O}_4 \cdot \text{H}_2\text{O}$  to remove any adherent salt particles, after which the total radioactivity of each sample was determined. A 2-min period was used for all count rate determinations.

The concentration profile of radiotracer in the loop wall was next determined using an electrolytic machining technique.<sup>15</sup> A teflon plug was pressed in one end of the specimen and the inside of the specimen was filled with electrolyte. The specimen, which served as a cathode, was then clamped in a vertically mounted lathe chuck and was turned around a graphite anode located concentric to the axis of the specimen. At specified intervals, the specimen was weighed and the radioactivity of both the specimen and electrolyte was determined. This process was repeated until less than 10 per cent of the original activity remained in the alloy. Again a 2-min counting period was used.

Diffusion coefficients were calculated on the basis of both the total specimen activities and on the radiotracer

concentration profiles determined by electropolishing.

Equation 7A, Appendix A, was used for the former calculation and equation 8A, Appendix A, for the latter.

#### Corrosion Experiment (Loop 1249)

A second INOR-8 loop incorporating Cr-51 was operated to determine the validity of the diffusion coefficients measured in Loop 1248 for the prediction of Cr diffusion rates under corrosive conditions. This loop, No. 1249, was identical in design to Loop 1248 and was operated under temperature conditions similar to those shown in Figure 4. Tracer-containing salt was circulated in this loop for a period of 792 hours to allow for the absorption of Cr-51 tracer by the loop walls. Following this "seeding" operation, an addition of 6720 ppm  $\text{FeF}_2$  was made to the loop without otherwise disturbing the salt or operating conditions. After 264 hours of additional operation under corrosive conditions, the loop was drained and examined. The methods of examination were exactly the same as those described for Loop 1248.

The data of the second loop were correlated using the following equations:

$$\frac{y}{z} = 2A \rho \frac{w_{\text{Cr}}}{w_{\text{Cr}^{++}}} \left( \frac{D}{\pi} \right)^{\frac{1}{2}} \left[ (t')^{\frac{1}{2}} - (t' - t_0)^{\frac{1}{2}} \right] \quad (15)$$

and

$$F(x) = \frac{100\sqrt{\pi} \left[ (t')^{\frac{1}{2}} \int_w^{\infty} \operatorname{erfc} w dw - (t' - t_0)^{\frac{1}{2}} \int_u^{\infty} \operatorname{erfc} u du \right]}{(t')^{\frac{1}{2}} - (t' - t_0)^{\frac{1}{2}}} \quad (16)$$

where

$y$  = total counts of the entire specimen per min at  $t$

$z$  = counts of the salt per gm per min at  $t$

$W$  = weight fraction

$F(x)$  = per cent of original activity remaining at penetration  $x$ , cm

$t'$  = total time of exposure

$t_0$  = time at which  $\text{FeF}_2$  was added

$$w = \frac{x}{2(Dt')^{\frac{1}{2}}}$$

$$u = \frac{x}{2[D(t' - t_0)]^{\frac{1}{2}}}$$

These equations are analogous to those for heat transfer in a semi-infinite flat plate, one surface of which is initially heated at a constant temperature and then is cooled at a constant temperature.<sup>16</sup> The flow of heat with time for this case is exactly analogous to the flow of tracer with time in the corrosion experiment described.

## CHAPTER V

### RESULTS AND DISCUSSION

#### I. EFFECTS OF ALLOYING ADDITIONS

The effects of alloying additions to Ni-Mo alloys were evaluated in terms of both the corrosion products entering the salt mixtures and the metallographic appearance of the alloy after test. Results have been grouped in this section according to each of the elements studied.

##### Chromium

Corrosion-product concentrations. Effects of Cr additions were investigated by means of loop tests of six Ni-Mo-Cr alloys with Cr contents of 3.2 to 11.0 atomic per cent. One loop of each of these compositions was operated with Salt 107 for 500 hours under the standard temperature conditions as described in Chapter IV. The compositions investigated and the attendant concentrations of Cr ions in salt samples taken at the conclusion of these tests are shown in Table V. The extent of reaction between Cr and fluoride constituents, as indicated by the Cr ion concentrations, varied markedly with the amount of Cr in the alloy. This variation is illustrated graphically in Figure 5, where the data are compared with data for Inconel<sup>17</sup> and for pure Cr.<sup>18</sup>

TABLE V  
CORROSION-PRODUCT CONCENTRATIONS OF SALTS TESTED WITH Ni-Mo-Cr ALLOYS

Heat No.	Alloy Composition (atomic %)		Test Duration (hr)	Cr Concentration in Salt Samples* (mole %)		
	Cr	Other Components		Sample H	Sample C	Other
OR 37A-1	3.20	13.5Mo, Bal Ni	500	0.0194	0.0180	0.0213
OR 30-1	3.41	11.1Mo, Bal Ni	500	0.0222	0.0365	0.0291
OR 30-2	5.55	10.8Mo, Bal Ni	500	0.0375	0.0352	0.0376
OR 30-2	5.55	10.8Mo, Bal Ni	1000	0.0509	0.0509	0.0543
OR 30-6	7.60	9.72Mo, Bal Ni	500	0.0606	0.0606	0.0566
OR 43A-3	7.71	13.4Mo, Bal Ni	500	0.0453	0.0476	0.0425
OR 30-4	11.04	10.6Mo, Bal Ni	500	0.0819	0.0814	0.0699

\*Sample designations "H" and "C" are discussed in Chapter IV, page 24; "Other" designates samples obtained from metallographic specimens.

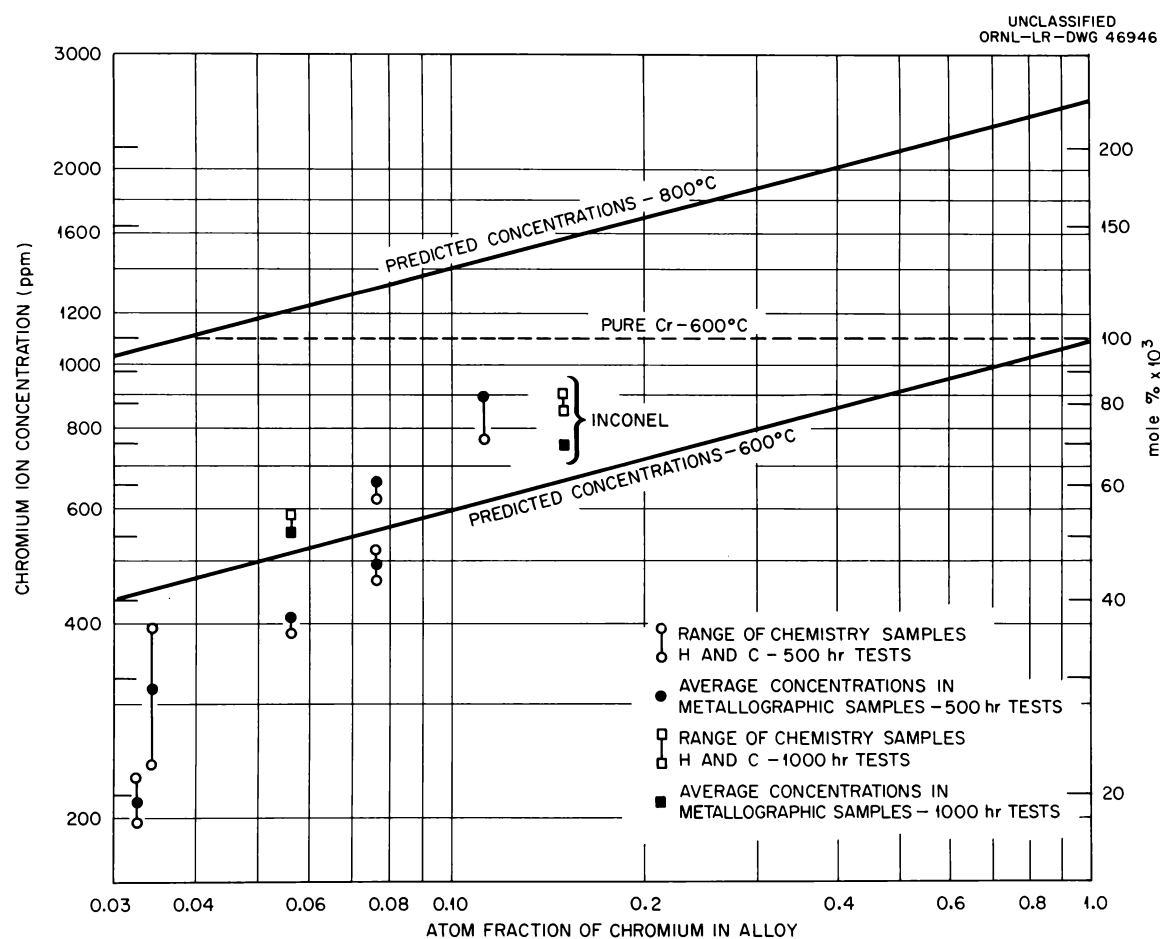


Figure 5. Concentration of Cr ions in Salt 107 as a function of Cr content in Ni-Mo-Cr alloys.

It may be noted that the Cr concentrations of the salts were less than those for Inconel loops operated under identical temperature conditions. A horizontal line, which represents the Cr ion concentration at equilibrium with pure Cr at 600°C, is seen in Figure 5 to be above the measured Cr ion concentrations for the alloys tested. Thus, the observed concentrations were less than those required for the formation of pure Cr crystals in the coldest portion of the loops (approximately 650°C).

As discussed in Chapter III, the concentration of Cr ions under the conditions of these tests should be governed by the relation (equation 14)

$$N_{Cr \text{ ions}} = (N_{CrF_2} * N_{CrF_3}) = K_2 \underline{\alpha}_{Cr}^{5/19}$$

where  $N_{Cr \text{ ions}}$  is the mole fraction of Cr ions in Salt 107 at equilibrium with an alloy of given Cr activity,  $\underline{\alpha}_{Cr}$ . If it is assumed that  $N_{Cr} = \underline{\alpha}_{Cr}$ , the resultant Cr ion concentrations plotted for these alloys in Figure 5 should lie within a region which is bounded above by the function determined at a temperature equivalent to the maximum loop temperature and below by the function determined at the minimum loop temperature. Bounds using experimental values of  $K_2$  measured at 800°C and 600°C (Table I), which reasonably approximate the maximum and minimum loop temperatures, are plotted in Figure 5 and are seen to include only two of the

observed loop concentrations, both corresponding to Cr compositions greater than 7 atomic per cent. However, except for the alloy with least Cr content, all concentrations lie relatively close to the lower bound and roughly approximate the slope of this bound.

The deviation of measured corrosion-product concentrations in these tests from the predicted concentration ranges may have resulted primarily from inaccuracy in the assumption that  $N_{Cr} = \alpha_{Cr}$ . However, assuming  $\alpha_{Cr}$  to be accurately known, the corrosion-product concentrations in these tests would nevertheless have been lower than those predicted, since corrosive attack would necessarily reduce the Cr content and hence the Cr activity at the surface of the alloys relative to the original Cr activity. Furthermore, it is possible that the test times were not sufficiently long for the Cr concentration of the salt to have completely attained the maximum or steady-state level. To evaluate this latter point, sufficient material of one of the alloy compositions, Heat No. OR 30-2, was obtained to permit the operation of a 1000-hr test. Results of this test, which are shown in Table V and Figure 5, indicated that only a small increase in Cr concentration occurred between the 500-hr and 1000-hr intervals. It was concluded, therefore, that the 500-hr test provided a reasonably close estimate of the limiting corrosion-product concentrations associated with the

temperature conditions of these experiments.

Additional data on the effects of Cr in Ni-Mo alloys were afforded by tests of five alloys which contained Cr in combination with one or more other alloying elements, as shown in Table VI. Notwithstanding the additional alloying agents, the concentrations of Cr-containing corrosion products following 500-hr tests of these alloys in Salt 107, as shown in Table VI, were comparable to the concentrations associated with the simple ternary Cr-containing alloys. The corrosion-product concentrations for the alloys with multiple additions are plotted in Figure 6, and are seen to show the same general variation with Cr content as the ternary alloys (see Figure 5).

Also shown in Table VI and Figure 6 are the results of 1000-hr tests of four of the alloys containing multiple additions. After all but one of these tests, the Cr ion concentrations in the salts were slightly higher than for 500-hr tests of the same alloys; in one test, the Cr ion concentration was unaccountably lower.

Cr ion concentrations after both time intervals in the case of these multi-component alloys again fell near those predicted on the basis of equilibrium data for pure Cr at 600°C and were considerably less than the concentration needed to deposit pure Cr at 600°C.

The Cr activities in all of the alloys tested would

TABLE VI

CORROSION-PRODUCT CONCENTRATIONS OF SALTS TESTED WITH Ni-Mo ALLOYS CONTAINING  
Cr IN COMBINATION WITH OTHER ALLOYING ELEMENTS

Heat No.	Alloy Composition (atomic %)		Test Duration (hr)	Cr Concentration in Salt Samples* (mole %)		
	Cr	Other Components		Sample H	Sample C	Other
OR 30-16	4.30	2.54Al, 1.90Ti, 10.2Mo, Bal Ni	500	0.0227	0.0236	0.0204
S T23011	4.79	1.27Al, 2.91Nb, 1.72W, 10.2Mo, Bal Ni	500	0.0490	0.0490	0.0426
OR 30-33	5.90	1.59Al, 5.56Fe, 9.66Mo, Bal Ni	1000	0.0689	0.0731	0.0620
OR 30-22	6.64	0.43Fe, 0.39Nb, 2.61Al, 10.05Mo, Bal Ni	500	0.0583	0.0555	0.0490
OR 30-22	6.64	0.43Fe, 0.39Nb, 2.61Al, 10.05Mo, Bal Ni	1000	0.0416	0.0402	0.0370
B3276	9.32	1.48Nb, 14.0Mo, Bal Ni	500	0.0615	0.0615	0.0578
B3277	9.47	1.57Nb, 3.06Al, 14.2Mo, Bal Ni	500	0.0698	0.0700	0.0624
B3277	9.47	1.57Nb, 3.06Al, 14.2Mo, Bal Ni	1000	0.0731	0.0657	0.0740

\*Sample designations "H" and "C" are discussed in Chapter IV, page 24;  
"Other" designates samples obtained from metallographic specimens.

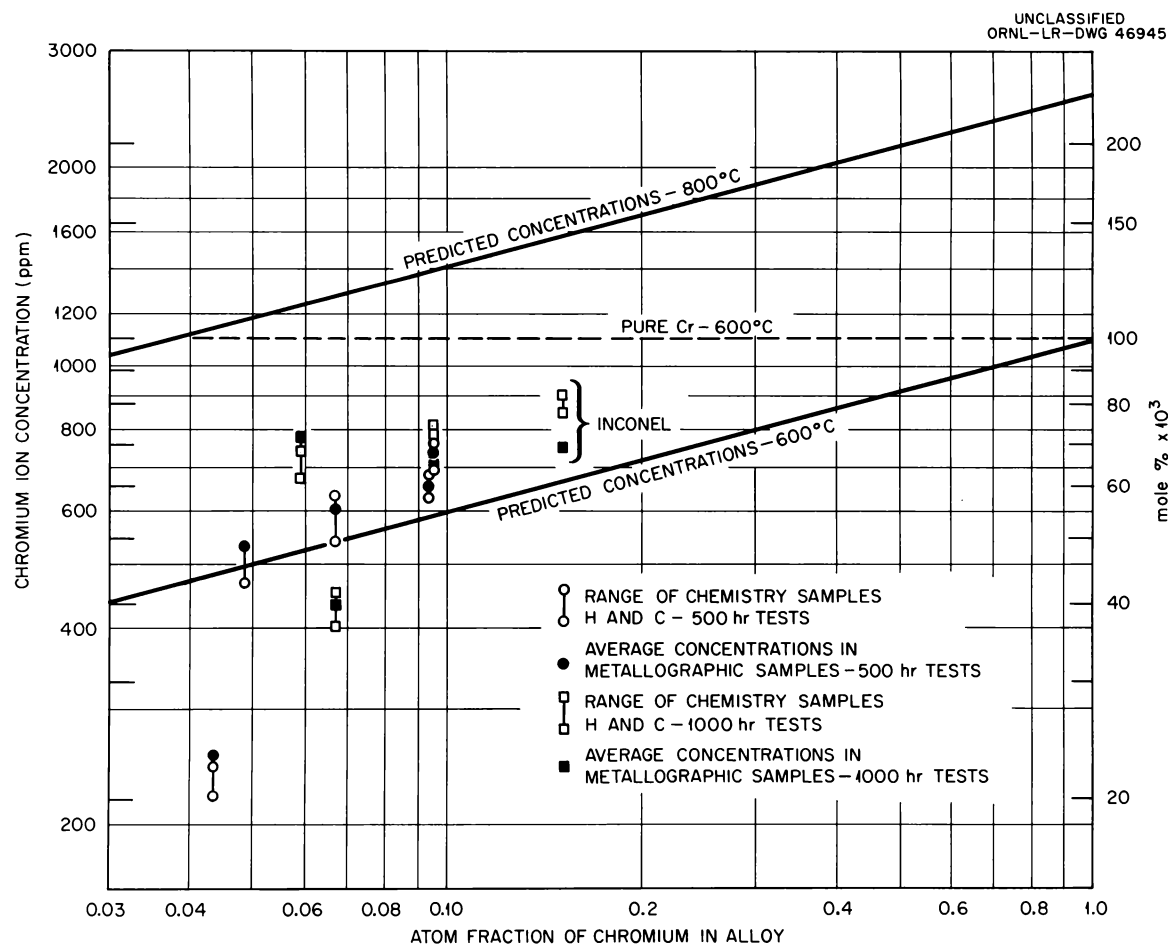


Figure 6. Concentration of Cr ions in Salt 107 as a function of Cr content in Ni-Mo alloys containing multiple alloy additions.

appear on the basis of corresponding corrosion-product concentrations to be lower than the activity of Cr in Inconel. However, it is important to note in Figures 5 or 6 that any alloy in which the Cr activity exceeded a value of 0.035 could support the formation of pure Cr at 600°C if the concentrations of  $\text{CrF}_2$  and  $\text{CrF}_3$  were equal to that in equilibrium with the alloy at temperatures of 800°C or above. Thus, unless the activity coefficients for Cr in these alloys are considerably less than one, the possibility for the deposition of pure Cr in cold-leg regions cannot be completely excluded for any of the alloys tested. In the case of  $\text{ZrF}_4$ - or  $\text{BeF}_2$ -base mixtures, as discussed in Chapter III, the temperature-dependence of the Cr- $\text{UF}_4$  reaction is much less than for Salt 107. It has been shown<sup>19</sup> that in these mixtures, alloys having a Cr activity equivalent to or less than that for Inconel cannot support Cr ion concentrations at 800°C which are sufficiently high to maintain pure Cr at 600°C. Consequently, mass transfer of Cr by deposition of pure Cr crystals in the latter salt mixtures should not be possible for any of the alloys listed in Tables V and VI.

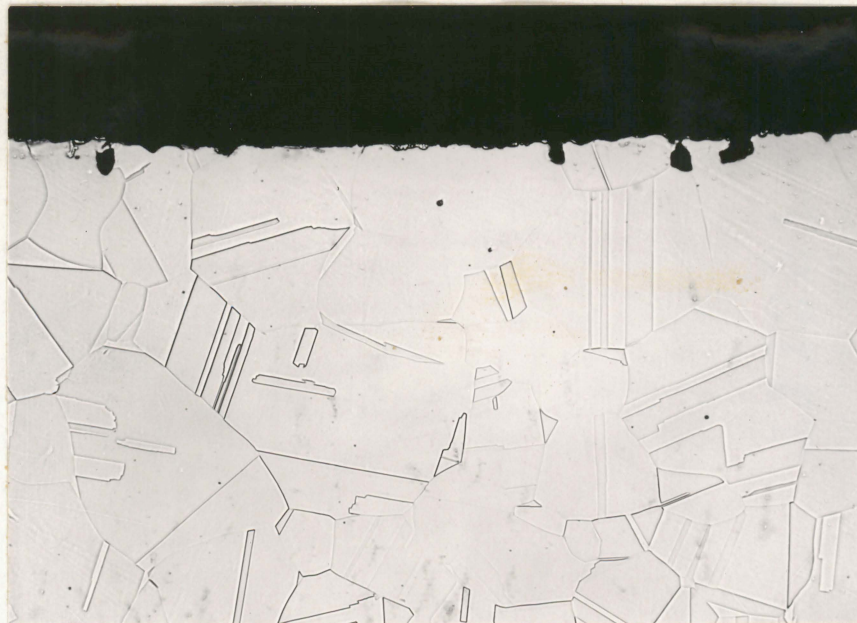
Metallographic results. Metallographic examinations of the ternary alloys shown in Table V showed little evidence of corrosive attack other than shallow surface roughening. Void formation, which characteristically had been found in

Ni-Cr alloys under similar test conditions,<sup>20</sup> was not detected in any of these alloys. The relative depths of attack which occurred for the alloy containing 5.55 atomic per cent Cr (Heat No. OR 30-2) after 500- and 1000-hr tests, respectively, are compared in Figure 7. Although the depth of attack was similar at both time intervals, the intensity of surface pitting was somewhat greater after the 1000-hr exposure. The intensity of surface roughening was also found to increase with increasing Cr concentration, as may be seen in Figure 8 which compares photomicrographs of two alloys containing different Cr contents. Cold-leg sections of these loops showed no evidence of corrosion and contained no visible deposits of corrosion products.

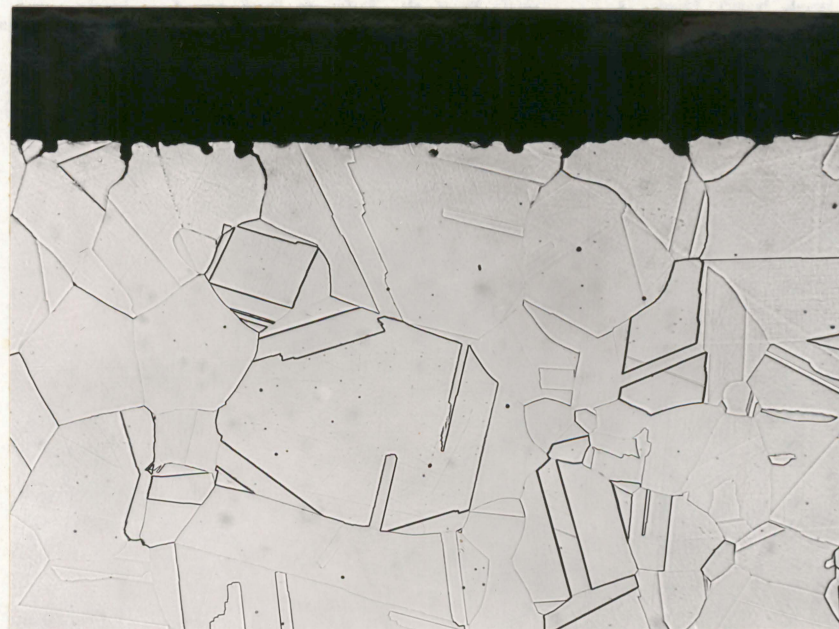
The depths of attack observed metallographically for alloys containing Cr in combination with other additions are shown graphically in Figure 9. Attack in these alloys was manifested as surface roughening after 500 hours and as a combination of surface pitting and shallow void formation after 1000 hours. Depths of corrosion were in general higher than for the ternary Cr-containing alloys, particularly in alloys which contained Al additions.

#### Aluminum

Corrosion-product concentrations. Table VII lists the concentrations of Al which were analytically determined

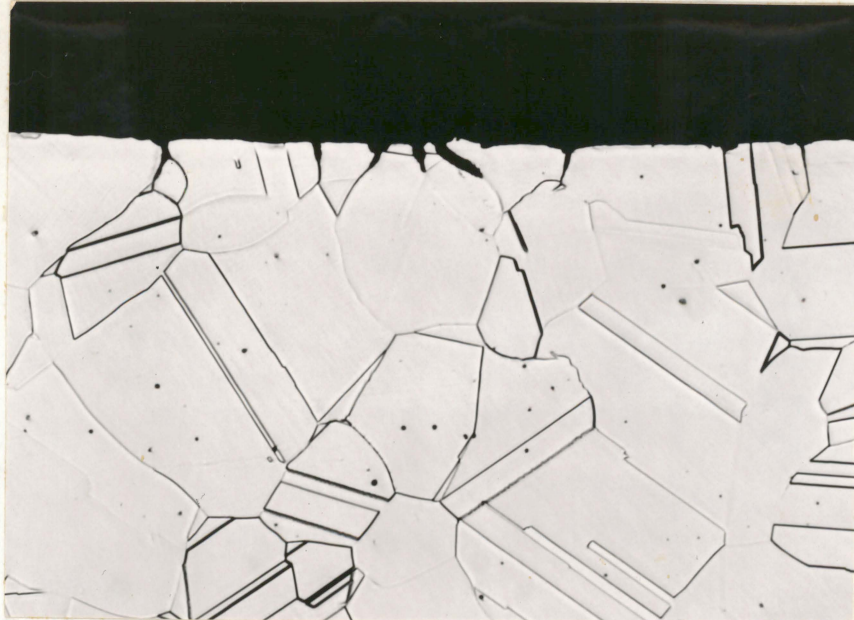


After 500 hr



After 1000 hr

Figure 7. Appearance of hot-leg surface of ternary Ni-Mo alloy containing 5.55 atomic per cent Cr following exposure to Salt 107. Heat No. OR30-2; 250X.



Composition: 3.2 Cr, 13.5 Mo, bal Ni (at. %)



Composition: 11.0 Cr, 10.6 Mo, bal Ni (at. %)

Figure 8. Hot-leg sections of Ni-Mo-Cr thermal convection loops following 500-hr exposure to Salt 107. 250X.

UNCLASSIFIED  
ORNL-LR-DWG 46944

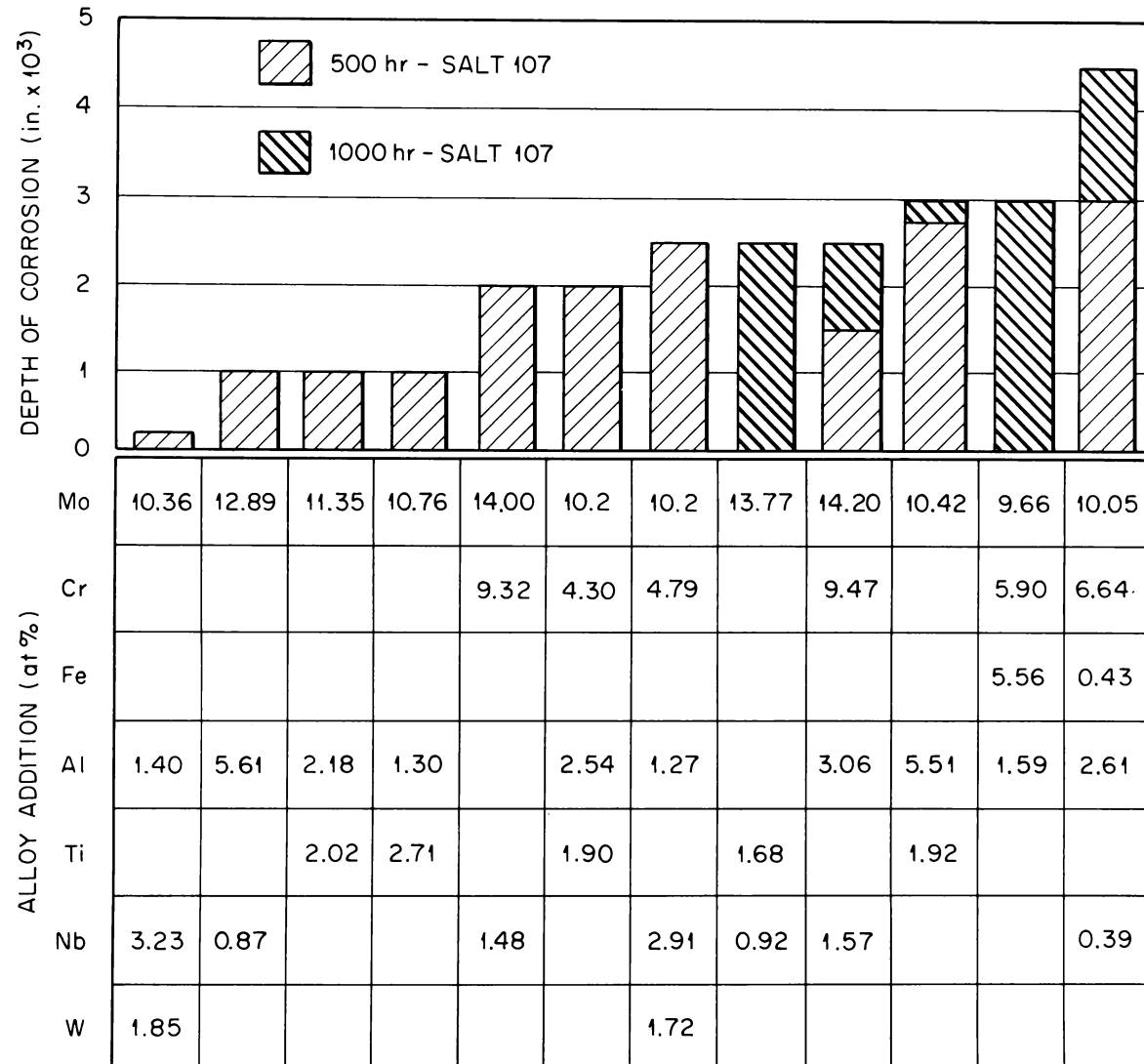


Figure 9. Depths of corrosion observed for Ni-Mo alloys with multiple alloy additions following exposure to Salt 107. Bars designating corrosion depths appear directly above the alloy compositions which they represent. (Where bars have both positively-sloped and negatively-sloped cross-hatching, the height of positively-sloped cross-hatching indicates depth of corrosion after 500 hr and combined height of both types indicates depth after 1000 hr.)

TABLE VII

## CORROSION-PRODUCT CONCENTRATIONS OF SALTS TESTED WITH Ni-Mo-Al ALLOYS

Heat No.	Alloy Composition (atomic %)		Test Duration (hr)	Al Concentration in Salt Samples* (mole %)		
	Al	Other Components		Sample H	Sample C	Other
S T23012	1.22	11.4Mo, Bal Ni	500	0.000872	0.000872	**
OR 30-7	4.26	10.15Mo, Bal Ni	500	0.220	0.070	0.137
OR 30-7	4.26	10.15Mo, Bal Ni	1000	0.214	0.105	0.178
OR 1491	4.85	6.99Mo, Bal Ni	1000	0.374	0.374	0.374

\*Sample designations "H" and "C" are discussed in Chapter IV, page 24; "Other" designates samples obtained from metallographic specimens.

\*\*Not determined.

in fluoride mixtures operated for 500- and 1000-hr periods with Ni-Mo alloys containing single additions of Al. In the case of alloys containing greater than 2 atomic per cent Al, the corresponding Al concentrations in the salt mixture were relatively high, i.e., in the range of 0.15-0.37 mole per cent. Only one alloy composition was subjected to tests at both 500 and 1000 hours; however, results for this alloy suggest that effectively similar salt concentrations were realized for both time intervals. Concentrations of corrosion products which formed in salt mixtures circulated in loops containing Al in combination with other alloying elements are shown in Table VIII. These concentrations were of the same general magnitudes as those observed for the ternary Ni-Mo-Al alloys.

The corrosion-product concentrations showed no definable correspondence with the Al content of the alloys. However, the propensity for Al to react with interstitial contaminants, such as N, in these alloys, makes the activity of Al in the alloys very dependent on composition and metallurgical history. For this reason, poor correspondence between the corrosion-product concentration and total Al concentration in the alloy would not be unexpected.

It is apparent from tests of both the ternary and multi-component alloys that Al additions less than 2 atomic per cent give rise to very much lower Al ion concentrations

TABLE VIII

CORROSION-PRODUCT CONCENTRATIONS OF SALTS TESTED WITH Ni-Mo ALLOYS CONTAINING  
Al IN COMBINATION WITH OTHER ALLOYING ELEMENTS

Heat No.	Alloy Composition (atomic %)		Test Duration (hr)	Al Concentration of Salt Samples* (mole %)		
	Al	Other Components		Sample H	Sample C	Other
S T23014	1.30	10.8Mo, 2.7Ti, Bal Ni	500	<0.0009	<0.0009	<0.0009
S T23013	1.40	10.4Mo, 3.2Nb, 1.8W, Bal Ni	500	0.160	0.0606	**
OR 30-33	1.59	9.7Mo, 5.9Cr, 5.6Fe, Bal Ni	1000	0.0660	0.0820	0.124
OR 30-16	2.54	10.2Mo, 4.3Cr, 1.9Ti, Bal Ni	500	0.358	0.326	0.334
OR 30-22	2.61	10.0Mo, 6.6Cr, 0.4Fe, 0.4Nb, 2.6W, Bal Ni	500	0.382	0.570	0.244
OR 30-22	2.61	10.0Mo, 6.6Cr, 0.4Fe, 0.4Nb, 2.6W, Bal Ni	1000	0.249	0.259	**
B3277	3.06	14.2Mo, 9.5Cr, 1.6Nb, 3.1W, Bal Ni	500	0.502	0.525	0.481
B3277	3.06	14.2Mo, 9.5Cr, 1.6Nb, 3.1W, Bal Ni	1000	0.473	0.394	0.374
OR 30-14	5.51	10.4Mo, 1.9Ti, Bal Ni	500	0.394	0.439	0.499
OR 30-14	5.51	10.4Mo, 1.9Ti, Bal Ni	1000	0.250	0.174	0.0960

\*Sample designations "H" and "C" are discussed in Chapter IV, page 24;  
"Other" designates samples obtained from metallographic specimens.

\*\*Not determined.

than additions above 2 atomic per cent. This observation may suggest that below a concentration of 2 atomic per cent the bulk of the Al addition has formed highly stable compounds with interstitial contaminants.

Metallographic results. Hot-leg surfaces of ternary alloys containing Al in amounts greater than 2 atomic per cent underwent relatively severe attack by Salt 107 in the form of surface pitting and subsurface void formation. Void formation was evident to a depth of 0.002 in. in 500-hr tests of these alloys and to 0.003 in. in 1000-hr tests. Figure 10 shows the appearance of an alloy containing 4.27 atomic per cent Al after a 1000-hr test exposure. However, an alloy containing only 1.22 atomic per cent Al revealed negligible attack after a 500-hr exposure to Salt 107.

Alloys containing Al combined with other alloying components also exhibited both surface pitting and subsurface void formation after exposure to Salt 107. The depths of attack for these alloys are shown graphically in Figure 9. Additions of up to 2 atomic per cent Al resulted in only light attack except in alloys where Cr additions were also present. Alloys which contained over 2.5 atomic per cent Al in combination with Cr or Ti revealed pronounced attack in the form of subsurface voids to depths ranging from 0.002 in. to 0.0045 in. Cold-leg sections of all loops were unattacked and contained no insoluble corrosion products.

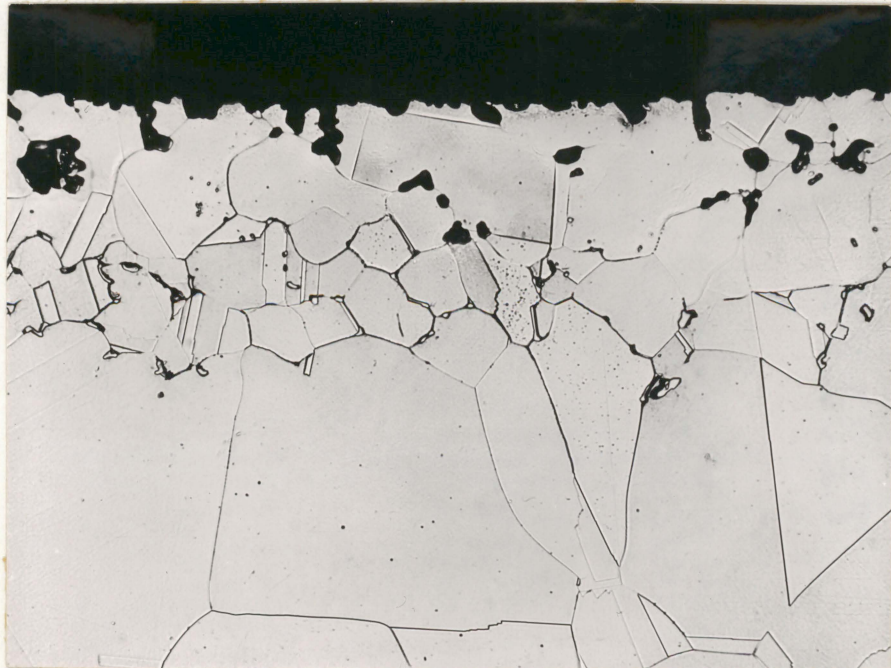


Figure 10. Hot-leg surface of ternary Ni-Mo alloy containing 4.27 atomic per cent Al after 1000-hr exposure to Salt 107. Heat No. OR30-7; 250X.

Titanium

Corrosion-product concentrations. Ti-containing alloys which were investigated are listed in Table IX, together with attendant Ti corrosion-product concentrations. Except for the first composition shown, which contained 2.47 atomic per cent Ti, alloying agents in addition to Ti were present in all of the alloys evaluated. The corrosion properties of the single ternary alloy were studied at both 500-hr and 1000-hr time intervals. Analyses of salts operated in loops of this alloy revealed Ti concentrations of 0.038-0.040 mole per cent after 500 hours and 0.040-0.055 mole per cent after 1000 hours. These analyses correspond closely to the analyses of salts circulated in loops constructed of the other Ti-bearing alloys, in which Ti contents ranged from 1.68 to 3.24 atomic per cent. Only the test of the 2.71 atomic per cent alloy effected a Ti salt concentration significantly different from the ternary alloy, the concentration in the former test being unaccountably lower than for the other tests.

Metallographic results. The ternary Ti-bearing alloy revealed only light attack in the form of surface pitting after both the 500-hr and 1000-hr test intervals. The photomicrograph in Figure 11 shows the appearance of a typical hot-leg section of this alloy after the longer test interval.

TABLE IX  
CORROSION-PRODUCT CONCENTRATIONS OF SALTS TESTED WITH  
Ni-Mo ALLOYS CONTAINING Ti

Heat No.	Alloy Composition (atomic %)		Test Duration (hr)	Ti Concentration in Salt Samples* (mole %)		
	Ti	Other Components		Sample H	Sample C	Other
OR 30-8	2.47	11.6Mo, Bal Ni	500	0.0394	0.0386	0.0380
OR 30-8	2.47	11.6Mo, Bal Ni	1000	0.0404	0.0495	0.0505
B2897	1.68	13.8Mo, 0.9Nb, Bal Ni	1000	0.0373	0.0383	0.0283
OR 30-16	1.90	10.2Mo, 4.3Cr, 2.5Al, Bal Ni	500	0.0378	0.0348	0.0500
OR 30-14	1.92	10.4Mo, 5.5Al, Bal Ni	500	0.0449	0.0489	0.0378
OR 30-14	1.92	10.4Mo, 5.5Al, Bal Ni	1000	0.0373	0.0530	0.0434
OR 30-13	2.02	11.3Mo, 2.2Al, Bal Ni	500	0.0389	0.0404	0.0484
S T23014	2.71	10.8Mo, 1.3Al, Bal Ni	500	0.0187	0.0242	0.0187
B2898	3.24	13.2Mo, 0.9 Nb, Bal Ni	500	0.0353	0.0252	**

\*Sample designations "H" and "C" are discussed in Chapter IV, page 24; "Other" designates samples obtained from metallographic specimens.

\*\*Not determined.

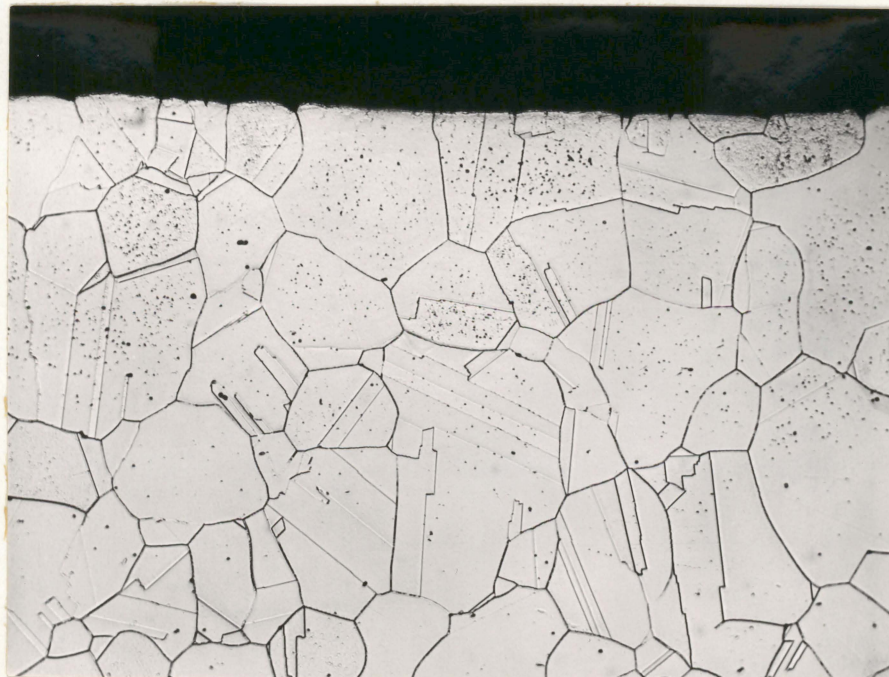


Figure 11. Hot-leg surface of ternary Ni-Mo alloy containing 2.47 atomic per cent Ti after 1000-hr exposure to Salt 107. Heat No. OR30-8; 250X.

Depths of attack which were observed in the remainder of the Ti-bearing alloys are graphically depicted in Figure 9. Except where Al additions were present in these alloys in amounts greater than 2 atomic per cent, depths of attack were in all cases less than 0.003 in. and generally were less than 0.002 in. Attack in all cases was manifested as general surface pitting and shallow void formation. No attack was seen in the cold-leg sections of any of the Ti-containing loops nor were cold-leg deposits detected.

#### Vanadium

Corrosion-product concentrations. Loops were operated with two ternary alloys containing V additions of 2.73 and 5.11 atomic per cent, respectively. As shown in Table X, the V concentration detected in a salt mixture tested with the former alloy after 500-hr exposure was less than 0.005 mole per cent. However, salts operated with the alloy of higher V content contained 0.027 mole per cent V in a 500-hr test and 0.019-0.020 mole per cent V in a 1000-hr test.

Metallographic results. Metallographic examination of the alloy with 2.73 atomic per cent V revealed very light attack in the form of surface roughening. Hot-leg surfaces of the alloy with 5.11 atomic per cent V exhibited attack in the form of void formation to a depth of 0.002 in. in the

TABLE X  
CORROSION-PRODUCT CONCENTRATIONS OF SALTS TESTED WITH  
Ni-Mo ALLOYS CONTAINING V AND Fe

Heat No.	Alloy Composition (atomic %)		Test Duration (hr)	Corrosion-Product Concentration in Salt Samples* (mole %)		
	V	Other Components		Sample H	Sample C	Other
<u>V Concentration</u>						
OR 30-10	2.73	10.8Mo, Bal Ni	500	<0.005	<0.005	<0.005
OR 30-20	5.11	10.8Mo, Bal Ni	500	0.0274	0.0274	0.0261
OR 30-20	5.11	10.8Mo, Bal Ni	1000	0.0198	0.0194	**
<u>Fe Concentration</u>						
OR 30-11	4.12	10.8Mo, Bal Ni	500	0.0146	0.0134	0.0152
OR 30-33	5.56	9.7Mo, 5.9Cr, 1.6Al, Bal Ni	1000	0.00517	0.00387	0.00517

\*Sample Designations "H" and "C" are discussed in Chapter IV,  
page 24; "Other" designates samples obtained from metallo-  
graphic specimens.

\*\*Not determined.

500-hr loop and 0.004 in. in the 1000-hr loop. A photomicrograph illustrating attack incurred by the latter loop is shown in Figure 12.

### Iron

Corrosion-product concentrations. Only two loop tests were completed with alloys containing Fe as a major addition. Results of both tests, one of which operated for 500 hours and the other for 1000 hours, are summarized in Table X. In the 500-hr loop, which contained 4.12 atomic per cent Fe, after-test salt samples were analyzed to contain 0.013-0.015 mole per cent of Fe. In the 1000-hr loop, which contained 5.56 atomic per cent Fe together with Al and Cr additions, the after-test salt samples contained an even lower Fe concentration. It would appear that corrosion products formed by reactions involving Cr and Al in this latter test served to inhibit the reaction with Fe.

Metallographic results. Metallographic examinations of specimens from the 500-hr loop showed no evidence of attack other than light surface roughening. Examinations of the 1000-hr test, as indicated in Figure 9, showed corrosive attack to a depth of 0.003 in. in the form of small subsurface voids.



Figure 12. Attack at hot-leg surface of ternary Ni-Mo alloy containing 5.11 atomic per cent V. Alloy was exposed to Salt 107 for 1000 hr. Heat No. OR 30-20; 250X.

Niobium

Corrosion-product concentrations. Loop tests of 500-hr and 1000-hr durations were carried out with ternary alloys containing 2.20 and 3.62 atomic per cent Nb, respectively. As shown in Table XI, the Nb concentrations in salts exposed to these alloys increased from a value near 0.015 mole per cent in the 500-hr tests to values of from 0.022 to 0.025 mole per cent in the 1000-hr tests. Salts tested with alloys which contained Nb combined with other additions showed very much lower Nb concentrations than did the simple ternary alloys. As seen in Table XII, concentrations in the multiple-addition tests were less than 0.002 mole per cent for Nb contents as high as 3.62 atomic per cent. Thus, it appears that corrosion products formed by reactions with other components in these alloys, namely Ti, Al, and Cr, were effective in inhibiting reaction of the salt with Nb.

Metallographic results. Neither ternary alloy containing Nb showed significant attack in metallographic examinations of 500-hr tests; however, the presence of very small subsurface voids to depths of approximately 0.001 in. was detected in examinations of the 1000-hr tests, as illustrated in Figure 13. Corrosion results determined for alloys containing Nb together with other additions are summarized in Figure 9. Except where Al and Cr were both present, attack

## CORROSION-PRODUCT CONCENTRATIONS OF SALTS TESTED WITH Ni-Mo-Nb ALLOYS

TABLE XI

Heat No.	Alloy Composition (atomic %)		Test Duration (hr)	Nb Concentration in Salt Samples* (mole %)		
	Nb	Other Components		Sample H	Sample C	Other
OR 30-12	2.20	11.1Mo, Bal Ni	500	0.00363(?)	**	0.0135
OR 30-12	2.20	11.1Mo, Bal Ni	1000	0.0225	0.0207	0.0233
OR 30-21	3.62	10.9Mo, Bal Ni	500	0.0155	0.0174	0.0153
OR 30-21	3.62	10.9Mo, Bal Ni	1000	0.0244	0.0228	0.0259

\*Sample designations "H" and "C" are discussed in Chapter IV, page 24; "Other" designates samples obtained from metallographic specimens.

\*\*Not determined.

TABLE XII

CORROSION-PRODUCT CONCENTRATIONS OF SALTS TESTED WITH Ni-Mo ALLOYS CONTAINING  
Nb IN COMBINATION WITH OTHER ALLOYING ELEMENTS

Heat No.	Alloy Composition (atomic %)		Test Duration (hr)	Nb Concentration in Salt Samples* (mole %)		
	Nb	Other Components		Sample H	Sample C	Other
OR 30-22	0.39	10.0Mo, 6.6Cr, 2.6Al, Bal Ni	500	0.00129	0.00181	0.00207
OR 30-22	0.39	10.0Mo, 6.6Cr, 2.6Al, Bal Ni	1000	0.00052	0.00104	0.00052
B2898	0.90	13.2Mo, 3.2Ti, Bal Ni	500	<0.0005	<0.0005	**
B2897	0.92	13.8Mo, 1.7Ti, Bal Ni	1000	0.00104	0.00052	0.00129
B3276	1.48	14.0Mo, 9.3Cr, Bal Ni	500	0.00078	0.00052	0.00078
B3277	1.57	14.2Mo, 9.5Cr, 3.1Al, Bal Ni	500	<0.0005	<0.0005	<0.0005
B3277	1.57	14.2Mo, 9.5Cr, 3.1Al, Bal Ni	1000	0.00259	0.00181	0.00104
S T23013	3.23	10.4Mo, 1.4Al, 1.8W, Bal Ni	500	<0.0005	<0.0005	<0.0005

\*Sample designations "H" and "C" are discussed in Chapter IV, page 24;  
"Other" designates samples obtained from metallographic specimens.

\*\*Not determined.

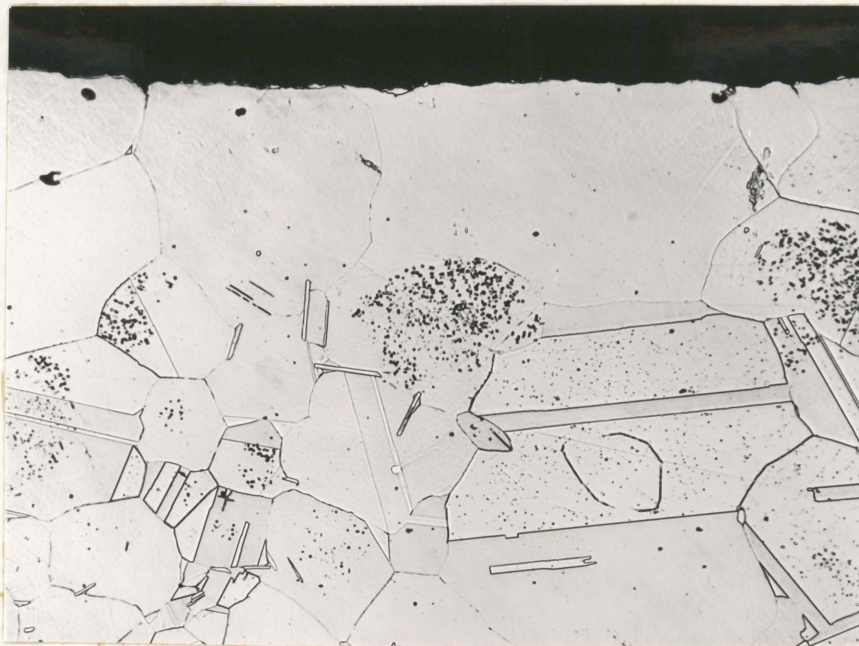


Figure 13. Appearance of voids in Ni-Mo alloy containing 3.62 atomic per cent Nb after 1000-hr exposure to Salt 107. Heat No. OR30-21; 250X.

in these alloys was less than 0.002 in. in depth.

Tungsten

Corrosion-product concentrations. Single alloying additions of W to the Ni-Mo system were evaluated at levels of 0.72 and 1.44 atomic per cent, respectively. Loop tests of both alloys were conducted for 500 hours, at which time W concentrations in the salt mixtures had reached levels of 0.029-0.032 mole per cent. In 500-hr tests of two alloys which contained W in addition to Cr, Nb, or Al, the concentrations of W detected in salt samples were below 0.010 mole per cent. Compositions of these alloys and their attendant salt corrosion-product concentrations are shown in Table XIII.

Metallographic results. Upon metallographic examination, loops constructed of Ni-Mo-W alloys revealed only slight surface pitting, as illustrated in Figure 14. An alloy containing W in combination with Al revealed heavy surface pitting, while an alloy containing W with Al, Cr, and Nb revealed subsurface voids to a depth of 0.0025 in., as shown in Figure 9.

TABLE XIII  
CORROSION-PRODUCT CONCENTRATIONS OF SALTS TESTED WITH  
Ni-Mo ALLOYS CONTAINING W

Heat No.	Alloy Composition (atomic %)		Test Duration (hr)	W Concentration in Salt Samples* (mole %)		
	W	Other Components		Sample H	Sample C	Other
OR 30-9	0.72	11.2Mo, Bal Ni	500	0.0318	0.0287	0.0325
OR 30-19	1.44	11.4Mo, Bal Ni	500	0.0384	0.0311	0.0310
S T23011	1.72	10.2Mo, 1.3Al, 2.9Nb 4.8 Cr, Bal Ni	500	0.00500	0.00983	**
S T23013	1.85	10.4Mo, 1.4Al, Bal Ni	500	0.00223	0.00105	**

\*Sample designations "H" and "C" are discussed in Chapter IV,  
page 24; "Other" designates samples obtained from metallo-  
graphic specimens.

\*\*Not determined.

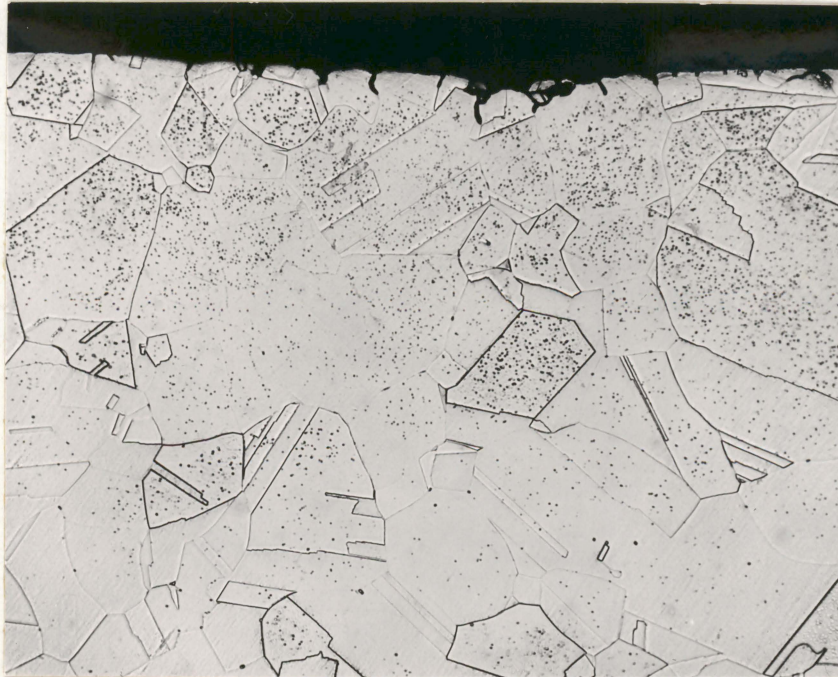
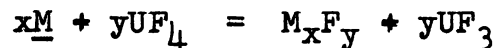


Figure 14. Hot-leg surface of Ni-Mo alloy containing 1.44 atomic per cent W after 500-hr exposure to Salt 107.  
Heat No. OR30-19; 250X.

Relative Thermodynamic Stabilities  
of Alloying Constituents

The salt mixtures supplied for the investigations of alloying effects on corrosion were extremely consistent in chemical composition. Accordingly, it may be supposed that the activities of  $\text{UF}_4$  and  $\text{UF}_3$  established at the start of each test were equally consistent. It follows, therefore, that the relative extent of reaction which occurred between the salt mixtures and an alloying element

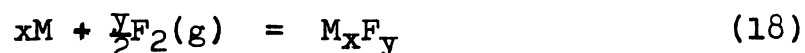


for which

$$K_a = \frac{a_{\underline{\text{M}}_x^F_y} \cdot a^y_{\text{UF}_4}}{a^x_{\underline{\text{M}}} \cdot a^y_{\text{UF}_3}} \quad (17)$$

can be related to the activity of the fluoride compound,  $\underline{\text{M}}_x^F_y$ , involving that element.

An indication of the relative activities of these compounds is provided by a consideration of their standard free energies of formation, as derived from the reaction



where

$$a_{\underline{\text{M}}_x^F_y} = e^{-\frac{\Delta F^\circ_T}{RT}}$$

In Table XIV are listed the standard free energies of formation, per gram-atom of F, of fluoride compounds at 800°C and

TABLE XIV  
 RELATIVE THERMODYNAMIC STABILITIES OF FLUORIDE COMPOUNDS  
 FORMED BY ELEMENTS EMPLOYED AS ALLOYING ADDITIONS  
 (Data compiled by Glassner)21

<u>Element</u>	<u>Most Stable Fluoride Compound</u>	$\Delta F^\circ$ $800^\circ C$ ( $\frac{\text{Kcal}}{\text{g. atom of F}}$ )	$\Delta F^\circ$ $800^\circ C$ ( $\frac{\text{Kcal}}{\text{g. atom of F}}$ )
Al	$\text{AlF}_3$	-87	-92
Ti	$\text{TiF}_3$	-85	-90
V	$\text{VF}_2$	-80	-84
Cr	$\text{CrF}_2$	-72	-77
Fe	$\text{FeF}_2$	-66	-66
Nb	$\text{NbF}_5$	-58	-60
W	$\text{WF}_5$	-46	-48

600°C associated with each of the alloying elements investigated. Values are given for the most stable compounds (i.e., those with most negative free energies) reported<sup>21</sup> for these elements, and are listed in order of decreasing stabilities. The resultant order suggests that corrosion-product concentrations associated with each element at a given activity should have increased in the following order: W, Nb, Fe, Cr, V; Ti, and Al.

In Figure 15, the general ranges of corrosion-product concentrations actually observed for these components, when present as single alloying additions, are plotted as a function of alloy content. It is seen that, with the exception of Nb and W, the concentrations per atomic per cent of addition do increase in the exact order predicted. Only W noticeably deviates from this predicted behavior; the causes for this deviation have not been established, although the number of tests completed on alloys with W additions were quite limited.

#### General Discussion of Alloying Effects

The corrosion-product concentrations associated with either Fe, Nb, or W alloying additions were much lower when these elements existed in multi-component alloys than in simple ternary alloys. The reason for this behavior is undoubtedly associated with the presence of the more reactive

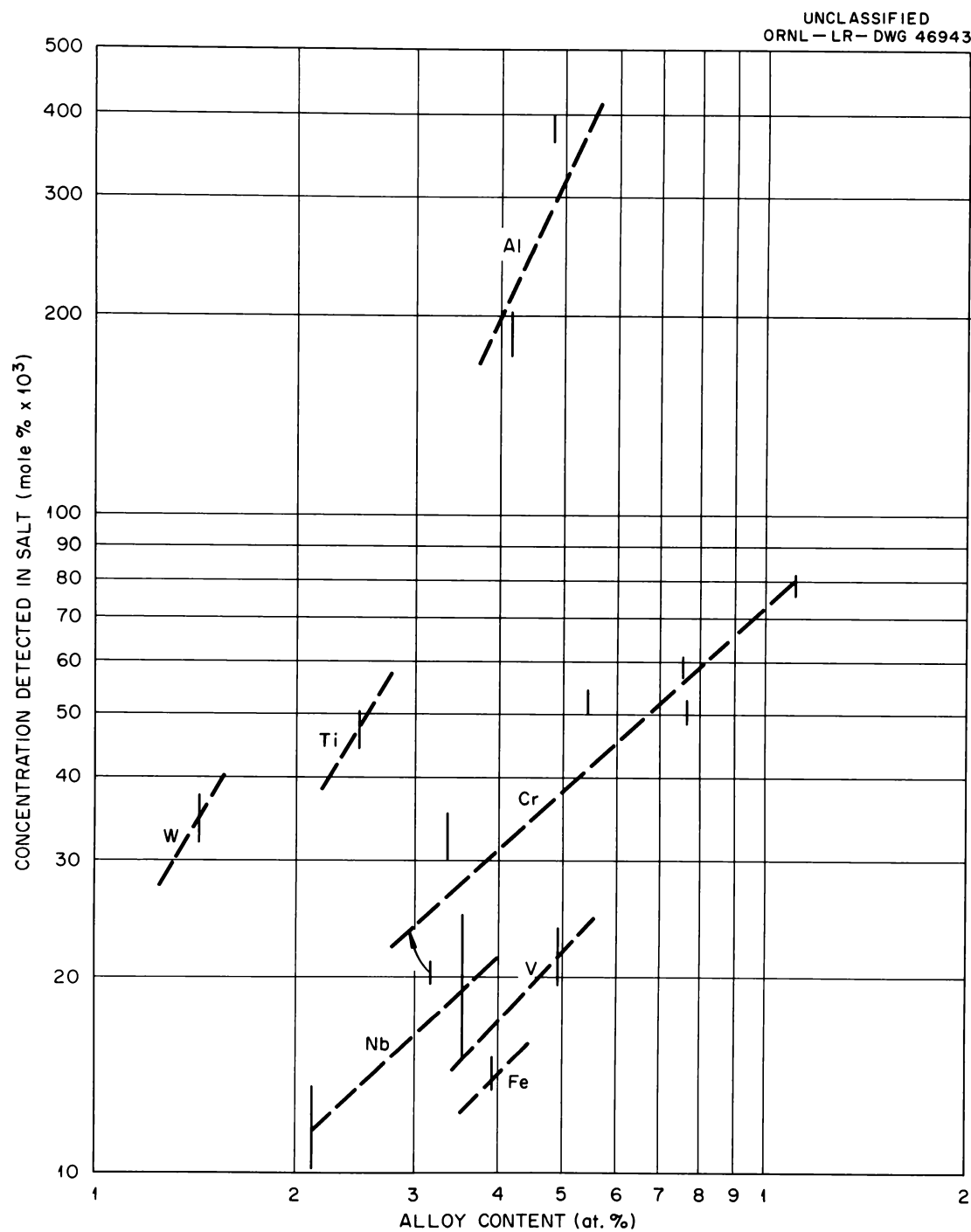
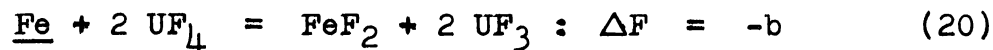
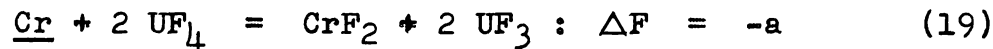


Figure 15. Comparison of corrosion-product concentrations formed in Salt 107 by various alloying additions as a function of alloy content.

alloying additions in the multi-component alloys. If one considers, for example, a system containing comparable additions of Cr and Fe, for which the corrosion reactions are



where

$$|a| > |b|$$

the equilibrium  $\text{UF}_3$  concentration produced by the first reaction is higher than that which would be produced by the second reaction. Accordingly, in the presence of Cr the  $\text{FeF}_2$  concentration at equilibrium will be reduced compared to the system containing Fe only.

While this means of corrosion inhibition was effective for those alloying components less reactive than Cr, its effect was not apparent among elements of relatively high reactivities. Thus, Cr corrosion-product concentrations were the same in the case of alloys containing both Al and Cr as in the case of alloys containing Cr alone. Similarly, the presence of Al did not noticeably reduce the Ti corrosion products associated with Ti-containing alloys. For most of the multi-component alloys, the amount of Cr and Ti, on an atomic per cent basis, exceeded that of Al; consequently their activities could have approached the activity of the Al component. Nevertheless, the high Al concentrations of fluoride mixtures after these tests

suggest a level of  $UF_3$  higher than would have been produced by either Cr or Ti alone, so that some inhibitive action would be predicted. The fact that none occurred may suggest that the measured Al concentrations were somewhat higher than actually existed.\*

The metallographic examinations of all alloys investigated under this program showed considerably less corrosion than Inconel under equivalent conditions. Surface roughening or shallow pitting was manifested in hot-leg sections of all the loops tested. Shallow subsurface voids were also seen in Al- and Nb-containing systems. Alloys containing more than one alloying addition invariably were attacked to depths greater than alloys containing each of the additions individually. The greatest depths of attack, which ranged from 0.003 in. to 0.0045 in. in 1000-hr exposures, were incurred in alloys which contained combined additions of Al and Cr or Al and Ti. Alloys without either Al or Ti in no case exhibited attack to depths of more than 0.002 in. and generally showed attack in the range from 0.001 in. to 0.002 in.

---

\*Considerable difficulty was in fact encountered in analyses of this element by wet chemical methods. Analyses of a limited number of samples were consequently made using semi-quantitative spectrographic techniques. Concentrations obtained by the latter technique were lower by a factor of approximately 2/3 than the values that were reported in Tables VII and VIII.

In the case of the majority of alloys tested, the rate of attack between 0 and 500 hours was substantially greater than the rate occurring between 500 and 1000 hours. This finding is in agreement with the concentrations of corrosion products, which in general increased only slightly between the periods of 500 and 1000 hours. Both results suggest that nearly steady-state conditions were established within the first 500 hours of test operation.

The favorable results of these tests permitted the consideration of the majority of potentially-useful alloying components in the selection of an optimum alloy composition. Only Ti and Al were felt to afford potential corrosion problems, particularly if used as combined additions or in combination with Cr. Because Cr had proved an extremely effective alloying agent in regard to both strength and oxidation improvements, this alloying addition was utilized for the selected container material, INOR-8. The level of Cr in this alloy was fixed at 7 per cent, which is the minimum amount required to impart oxidation resistance to the Ni-17 per cent Mo system.<sup>22</sup> The addition of Cr as an Fe-Cr alloy also imparted approximately 5 per cent Fe to the system. While the INOR-8 alloy was not tested as part of the initial alloy study, its corrosion properties can be considered equivalent to those of the ternary Cr-containing alloys discussed above.

## II. CORROSION PROPERTIES OF INOR-8

The materialization of INOR-8 as a container material for fluoride salt reactors focused further corrosion studies on this specific composition. The corrosive action of fluoride salts on this alloy, as would be expected, was selective and involved primarily the Cr constituent. Consequently, the corrosion rates in the alloy were allied with the rates at which Cr atoms diffused to surfaces undergoing corrosion. It was difficult in this case to relate the extent of corrosive damage to weight-loss or decrease in wall thickness, since these criteria failed to provide a measure of the extent and distribution of alloy depletion in zones beneath the exposed surfaces. Unfortunately, the affected areas were relatively shallow, so that analysis by chemical methods was also precluded. However, the use of radiotracers afforded a tool by which both the diffusivities of the affected element in the alloy and the rate of passage of the element out of the metal could be measured. Accordingly, the chemical composition of the alloy could be determined as a function of depth even though the affected areas were extremely shallow.

The results of measurements of Cr diffusivities in INOR-8 using these radiotracer techniques are outlined in this section. Also presented are the results of a test

operated to verify experimentally the corrosion rates and concentrations of depleted areas predicted by these diffusivities.

Radiotracer Diffusion Experiment (Loop 1248)

Diffusivity measurements. Measurements of the diffusion coefficients (diffusivities) of Cr in INOR-8 were provided by the operation of a single thermal convection loop experiment constructed of INOR-8 and exposed to a circulating fluoride mixture containing the radiotracer Cr-51, as described in Chapter IV. Fifteen specimens, representing 15 distinct temperature levels within the loop, were removed following operation, and the count rates of each specimen were recorded over a 2-min period to determine the amount of radioactive atoms present. By means of equation 7A in Appendix A, a Cr diffusion coefficient for each specimen and its corresponding temperature were computed on the basis of total radioactivity in the specimen and the time of exposure. The coefficients calculated by this method are shown as open triangles in Figure 16. Tables listing values of diffusivities and the measured radioactivity levels and other experimental data from which diffusivities were derived are contained in Appendix B.

Diffusion coefficients for Cr in these specimens were also determined from measurements of the tracer concentration

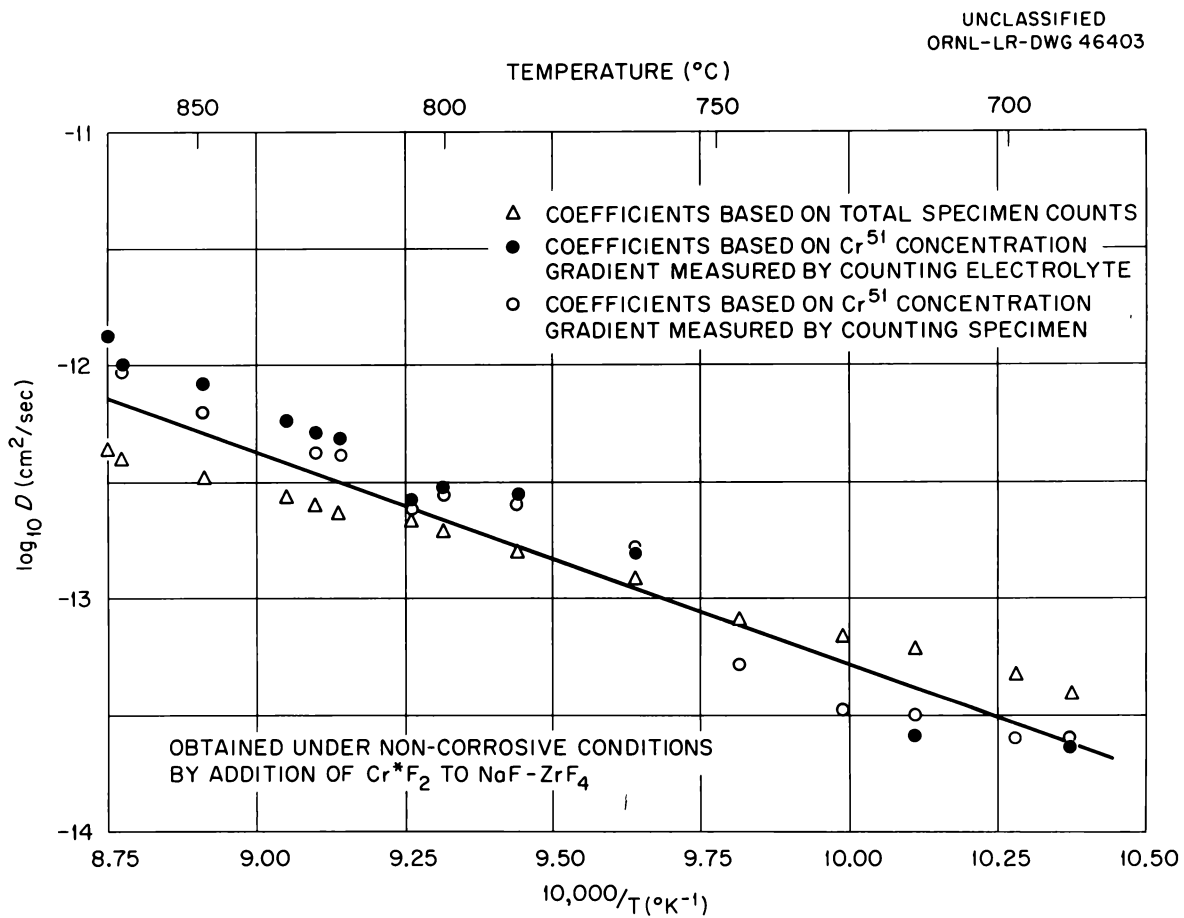


Figure 16. Relation between temperature and Cr-51 diffusion coefficients determined in INOR-8 Loop 1248.

profile beneath surfaces of the loop which had been exposed to salt. Successive layers were removed from these surfaces by electropolishing, and the radioactivity of each layer was determined by counting the electrolyte and by measuring the radioactivity loss in the specimen during each polishing. By means of these data, the percentage of radioactivity remaining after each polishing operation was established as a function of distance from the surface. Values of D were then computed for several distances below the surface using equation 8A in Appendix A. The arithmetic average of these values, which are shown for a typical specimen in Table XVIII, Appendix B, was then used to arrive at the functional relationship shown in Figure 17. Deviation of the experimental data from the derived curve is significant only for values of the ordinate below 10 per cent. This observation was found to hold for all of the test specimens examined.

A comparison of the D values obtained by the two methods described is shown in Figure 16. It is seen that at the higher temperatures, points based on the concentration profiles lie above those based on total specimen counts, while at lower temperatures the opposite is true. All points, however, are well within the over-all experimental precision, estimated to be  $\pm 0.4$  of a cycle.<sup>23</sup>

Values of the diffusivities of Cr in INOR-8, averaged as the straight line shown in Figure 16, compare rather

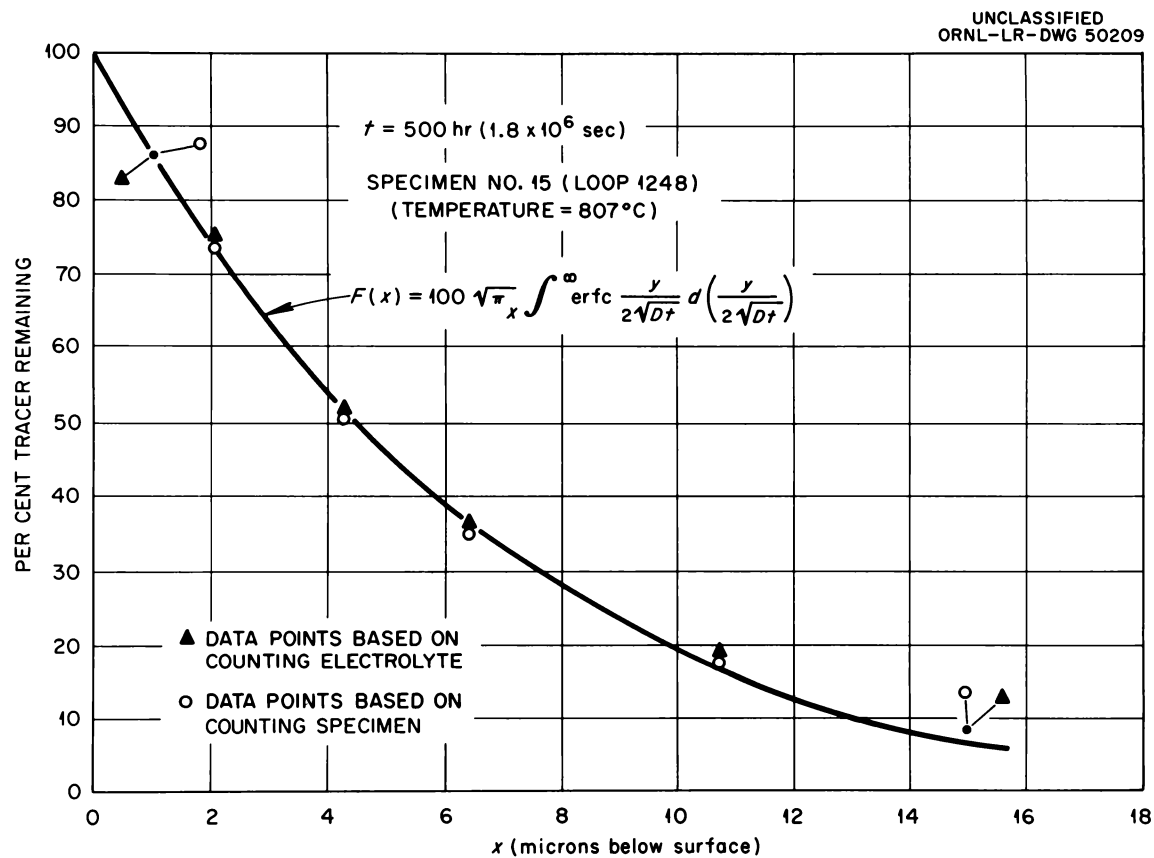


Figure 17. Per cent of Cr tracer remaining as a function of depth of removal from surface of specimen No. 15, Loop 1248. (The derived curve is based on the arithmetic average of D values computed from the data points shown.)

closely to similar data which have been published for the diffusion rate of Cr in Ni alloys. Generalized plots of Cr diffusivities for coarse- and fine-grained Inconel, which were obtained by Evans, et al.,<sup>24</sup> using the capsule technique described in Appendix A, are compared with values for INOR-8 in Figure 18. Also shown in Figure 18 are the values of Cr diffusivities reported in the literature for a Ni-based Cr alloy as determined at higher temperatures using a more conventional radiotracer technique.<sup>25</sup>

In order to verify that non-corrosive conditions were maintained during the operation of Loop 1248, sections of the loop adjacent to each of the diffusion specimens were examined metallographically. The appearance of the loop surface before test is compared in Figure 19 with a section removed from the point of maximum loop-wall temperature. The complete absence of corrosive attack in the latter specimen, as well as in other metallographic specimens removed from the loop, confirmed that the postulated non-corrosive conditions were closely realized.

Significance of diffusion coefficients. As discussed in Appendix A, the equations with which the data for the Loop 1248 experiment were correlated are based on a single phenomenological diffusion coefficient, as would be used to represent a homogeneous bulk diffusion process taking place in an

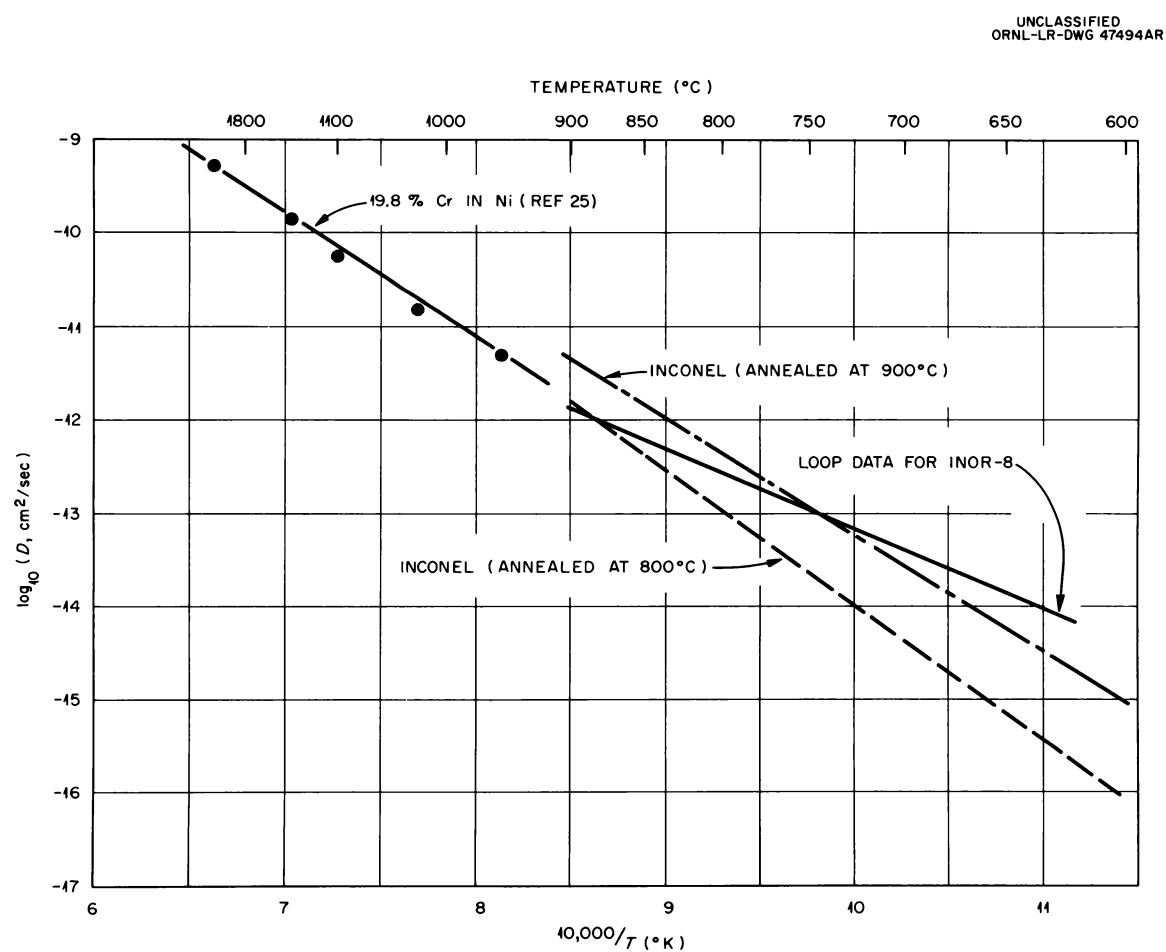


Figure 18. Comparison of diffusion coefficients for Cr in Ni-base alloys.



As-Received INOR-8 Tubing



Hot-Leg Surface after 500-hr

Figure 19. Comparison of surfaces of INOR-8 Loop 1248 before and after exposure to NaF-ZrF<sub>4</sub> salt containing Cr<sub>51</sub>F<sub>2</sub>. 250X.

isotropic medium. In polycrystalline materials, such as the INOR-8 specimens used for this experiment, however, there is a contribution due to grain-boundary diffusion. Theoretical treatments of such cases by Fisher<sup>26</sup> and Whipple<sup>27</sup> revealed that the time dependence of the penetration relationships would be altered when both mechanisms are combined. However, an analysis by Evans, et al.,<sup>28</sup> for diffusion in Inconel indicated that under the time and temperature conditions of the present experiment, grain-boundary diffusion would be of major importance only in the portion of the tracer profile curves corresponding to less than 10 per cent of the tracer remaining. As was noted previously, a deviation of data points from the profile curve based on an average diffusivity (Figure 17) was encountered only where the remainder of tracer fell under 10 per cent.

#### Radiotracer Corrosion Experiment (Loop 1249)

The data of Loop 1248 afforded a basis for impounding a known quantity and concentration gradient of Cr tracer in any INOR-8 loop system through exposure to tracer-containing salt. Since this exposure did not alter the original loop composition, it was possible by this means to produce an ideal system from which to initiate a corrosion experiment and trace the movement of Cr by means of the tagged atoms. Thus, Loop 1248 served as the control experiment for the

operation of a second INOR-8 radiotracer test, Loop 1249, which was intended to evaluate the validity of predicted Cr diffusion rates and alloy depletion profiles under corrosive conditions.

The applicability of the diffusion coefficients of Loop 1248 for the prediction of INOR-8 corrosion rates depended on two primary assumptions:

1. The corrosion rates were limited by the diffusion rates of Cr to loop surfaces undergoing depletion.

2. Diffusion coefficients calculated at the Cr concentration level of INOR-8 were valid despite changes in Cr concentration caused by corrosive attack.

To check the validity of these assumptions, Loop 1249 was exposed to Cr tracer under the same non-corrosive conditions used in Loop 1248. A corrosive agent,  $\text{FeF}_2$ , was then added without otherwise disturbing the operating conditions. The addition of  $\text{FeF}_2$ , a strong oxidant with respect to Cr, was intended to reduce the total Cr concentration at the surface to essentially zero.\* Moreover, it was not expected that this addition would affect the other components of INOR-8. Following the addition of  $\text{FeF}_2$ , the loop was operated for 264 additional hours and then was quickly drained. Fifteen specimens

---

\*The equilibrium constant for the reaction  $\text{Cr} + \text{FeF}_2 = \text{CrF}_2 + \text{Fe}$  is  $1.5 \times 10^4$  at  $600^\circ\text{C}$  and is greater at higher temperatures.

were again removed for examination at positions corresponding to those examined from Loop 1248.

Diffusivity measurements. Initial determinations of the diffusivities of Cr under these corrosive conditions were made on the basis of equation 15 in Chapter IV, which related an "overall" diffusion coefficient to the total specimen radioactivity. The concentration profile of each specimen was next determined by electropolishing, which allowed diffusivities to be derived using equation 16 in Chapter IV. Results of both methods are shown in Figure 20, together with the average data for Loop 1248. Data from which these diffusivity determinations were made and the corresponding diffusivities are presented in Appendix B.

Despite the change in total Cr concentration which occurred across the diffusion zone in Loop 1249, the diffusivities calculated on the basis of total specimen counts compared closely with the average diffusivities calculated for Loop 1248. Diffusivities based on measurements of the tracer concentration profiles, however, lay slightly above the data for Loop 1248. The concentration profile curve for a specimen from Loop 1249 exposed at 813°C is shown in Figure 21. The curve represents a plot of the theoretical profile function (equation 16) derived for the boundary conditions of the experiment, and is based on an average diffusivity value.

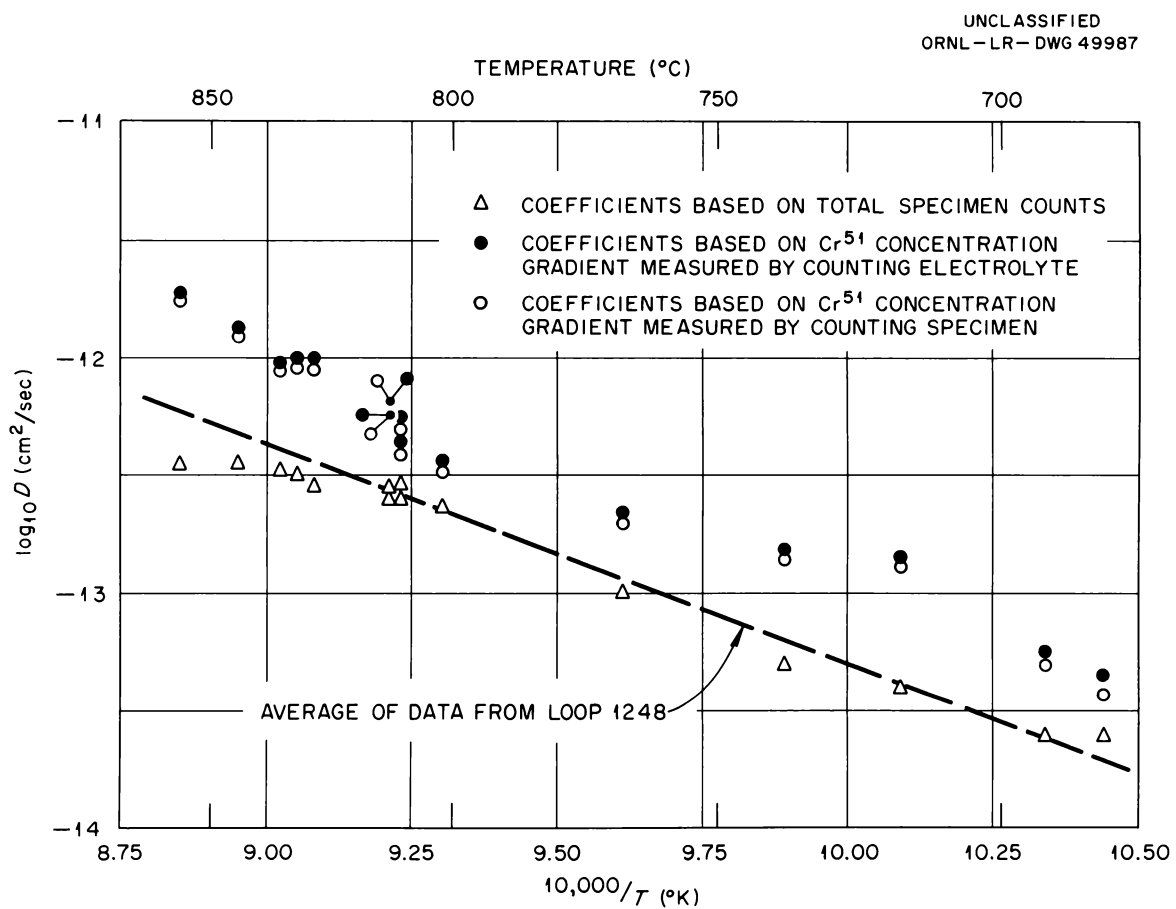


Figure 20. Relation between temperature and Cr-51 diffusion coefficients determined in INOR-8 Loop 1249.

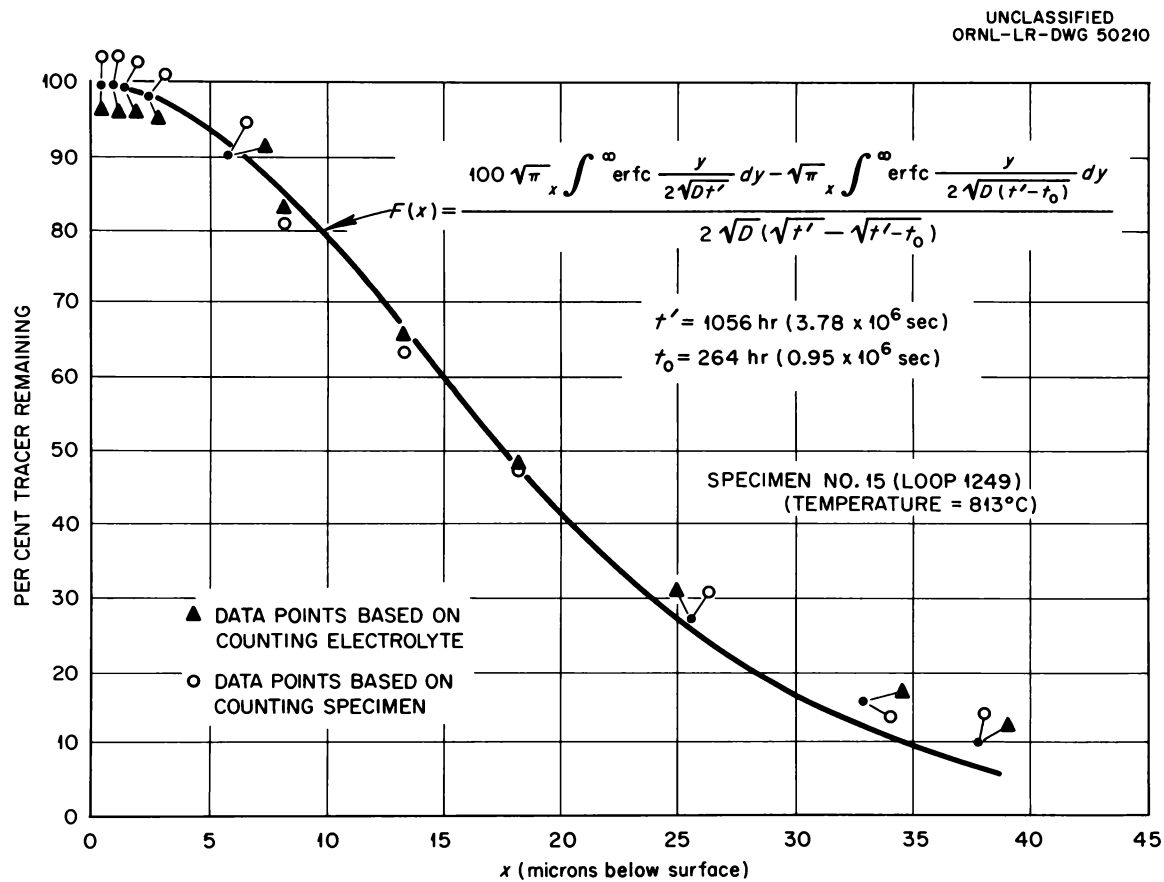


Figure 21. Per cent of Cr tracer remaining as a function of depth of removal from surface of specimen No. 15, Loop 1249. (The derived curve is based on the arithmetic average of D values computed from the data points shown.)

It will be noted that this single diffusivity establishes excellent concurrence between the function and all experimental points except those corresponding to relatively low percentages of tracer remaining in the specimen. This concurrence would not be expected if the diffusivity changed measurably as a function of Cr concentration.

In view of the similarity of diffusivities calculated on the basis of total radioactivity in specimens from Loops 1248 and 1249, it appeared that the overall amount of tracer which entered and which was removed from specimens in Loop 1249 compared exactly with that predicted by diffusion rates from Loop 1248. However, the distribution of tracer in Loop 1249 was such that higher diffusivities than for Loop 1248 were calculated from analyses of the concentration profiles. The reason for this discrepancy is believed to be associated with grain-boundary effects.

Grain-boundary effects, based on the extent of deviation of data points from the generalized profile curves at higher penetration depths, were more predominant in Loop 1249 than in Loop 1248. This observation is understandable considering that the ratio of tracer contained relatively deep in the alloy to the total amount of tracer present was lower for Loop 1248 than for Loop 1249. Thus, in the case of Loop 1249, the distribution of tracer relatively deep in the alloy was affected significantly by grain-

boundary diffusion and made a substantial contribution to the concentration profile curves. It is important to note that these curves were based on the percentage of tracer remaining in the specimen. In the case of Loop 1248, the contribution was relatively small except at percentages below 10 per cent. Since the rates of diffusion along grain boundaries invariably are higher than rates for volume diffusion, values of the apparent diffusivities should be increased correspondingly as grain-boundary effects become important.

These effects were of less importance in calculations of diffusivities based on total specimen radioactivity, since the latter calculations reflected the total amounts of tracer which entered the specimen and the total amounts withdrawn. In each case the bulk of the total amounts were made up of atoms close to the surface, where volume diffusion effects were predominant.

Corrosion rates. In view of the similarity of Cr diffusion coefficients calculated for Loops 1248 and 1249, it was evident that corrosion rates predicted for Loop 1249 on the basis of data from Loop 1248 should agree closely with measured corrosion rates. The agreement expected is demonstrated in Figure 22 which compares the extent of tracer depletion observed for a specimen from Loop 1249 with that predicted using the diffusivity measured in a specimen at a

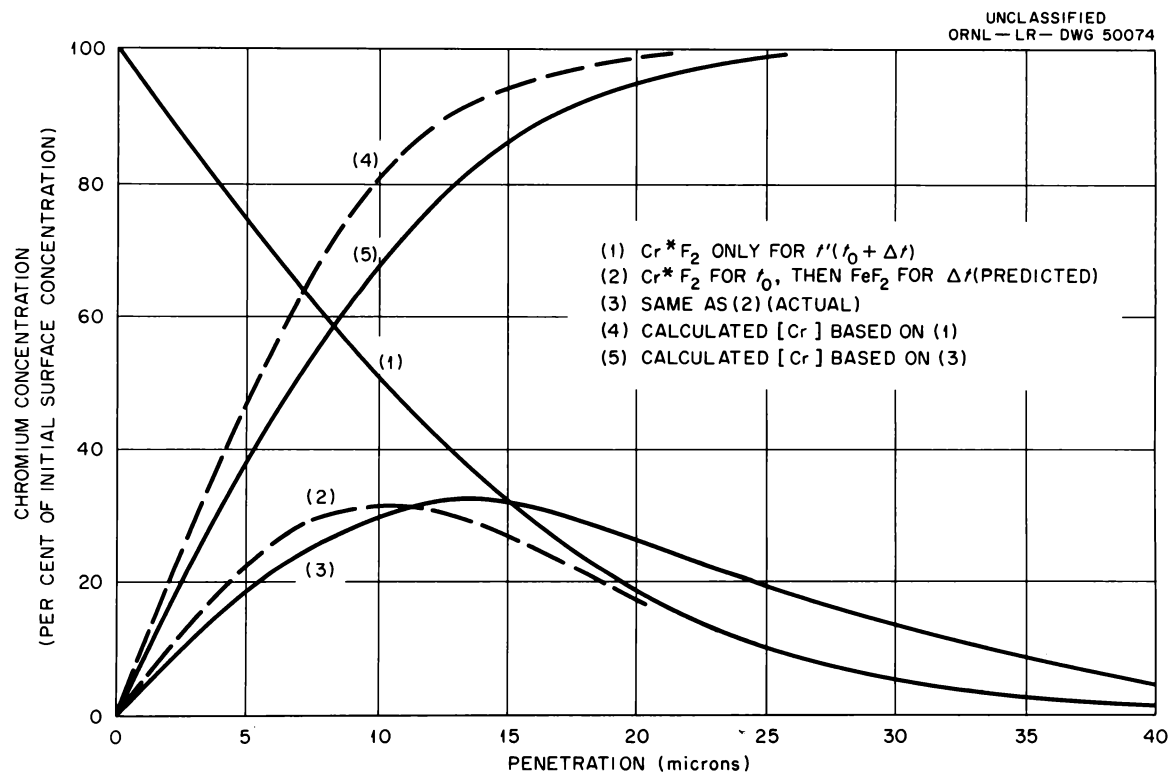


Figure 22. Comparison of predicted and actual Cr concentration profiles in specimen No. 15, Loop 1249. Curves (1) and (2) show Cr-51 (Cr\*) concentration profiles estimated on the basis of Cr diffusivities determined in Loop 1248. Curve (1) illustrates the concentration profile which should have resulted had non-corrosive conditions been maintained throughout the operation of Loop 1249. Curve (2) illustrates the profile predicted under the corrosive conditions imposed by the addition of FeF<sub>2</sub>. Curve (3) shows the actual (observed) Cr-51 concentration profile. Concentration profiles for total Cr atoms are shown in curves (4) and (5). Curve (4) is calculated on the basis of Cr-51 diffusivities measured in Loop 1248 under non-corrosive conditions. Curve (5) is calculated on the basis of the Cr-51 diffusivity determined from curve (3).

similar temperature position in Loop 1248. Curve (1) in Figure 22 shows the predicted concentration of tracer which would have existed in the specimen at the conclusion of the test if the  $\text{FeF}_2$  addition had not been made, i.e., under non-corrosive conditions. Curves (2) and (3) represent the predicted and observed tracer concentrations, respectively, following the 264-hr exposure to the salt containing  $\text{FeF}_2$ . The latter concentrations were derived by means of the functions\*

$$\frac{[C(\text{Cr-51})]_{t=t'} - [C(\text{Cr-51})]_{x=0}}{[C(\text{Cr-51})]_{x=0}} = \operatorname{erf} \frac{x}{2\sqrt{D(t'-t_0)}} - \operatorname{erf} \frac{x}{2\sqrt{Dt'}} \quad (21)$$

$0 \leq t \leq t_0$

where

$C$  = concentration in  $\text{g/cm}^3$

$t'$  = total time of loop operation

$(t' - t_0)$  = duration of  $\text{FeF}_2$  exposure (264 hr)

and accordingly are shown as the per cent of the surface concentration of tracer which existed prior to the  $\text{FeF}_2$  addition.

Diffusivities determined in each loop experiment were applied in a similar manner to calculations of the concentration profile and depletion of all Cr atoms for this specimen. Under the condition of constant surface concentration, i.e.,

\*This function is the differential form of the equation corresponding to the curve shown in Figure 21.

$[C_{Cr}]_{x=0} = 0$ , which was effected by the  $FeF_2$  addition, the concentration of Cr atoms at any depth,  $x$ , is given by the expression:

$$[C(x)]_{t=t'} = C_o \operatorname{erf} \frac{x}{2\sqrt{D(t'-t_o)}} \quad (22)$$

where

$C_o$  = initial Cr concentration of INOR-8 ( $g/cm^3$ )

Curves (4) and (5) in Figure 22 show the concentration of Cr, in terms of the per cent of initial Cr concentration, as predicted by this expression using the diffusivities obtained from Loops 1248 and 1249,\* respectively. It is apparent that the extent of Cr depletion predicted by data from Loop 1248 is slightly less than that predicted from the observed movement of tracer in Loop 1249.

The appearance of the corrosive attack produced in Loop 1249 by the  $FeF_2$  addition can be seen in Figure 23, which shows photomicrographs of the hottest and coldest sections of this loop. Attack in the former section, which operated at a temperature of  $857^\circ C$ , occurred as both concentrated surface pitting and shallow subsurface void formation. In the lower-temperature section, which operated at  $684^\circ C$ ,

\*The diffusivity used in the case of Loop 1249 was that based on the concentration profile of tracer rather than the total sample radioactivity. Had the latter diffusivity value been used, the Cr depletion curve would have been identical to that predicted by Loop 1248.



Cold-Leg Section ( $684^{\circ}\text{C}$ )  
Corrosion Rate:  $0.14 \text{ mg/cm}^2$



Hot-Leg Section ( $857^{\circ}\text{C}$ )  
Corrosion Rate:  $0.92 \text{ mg/cm}^2$

Figure 23. Appearance of cold- and hot-leg sections  
of Loop 1249 after exposure to  $\text{NaF-ZrF}_4$  salt containing  
 $\text{FeF}_2$ . 250X.

attack was much less severe, appearing as lightly concentrated surface pitting. Using the Cr diffusivities which had been calculated for these respective loop positions (based on the concentration profile), computations were made of the comparative amounts of Cr removed per sq cm in each of the sections. The relation used for these computations was of the form:

$$\Delta M = \int_0^\infty [C_o - C(x)] dx = \frac{2}{\sqrt{\pi}} \sqrt{D(t' - t_o)} C_o \quad (23)$$

The extent of Cr removal over the 264-hr test period was calculated to be  $9.2 \times 10^{-4}$  g/cm<sup>2</sup> in the case of the higher temperature specimen and  $1.4 \times 10^{-4}$  g/cm<sup>2</sup> in the case of the lower temperature specimen.

The removal of Cr as a consequence of oxidation by FeF<sub>2</sub> was seen by equation 3 to release a nearly equivalent amount of metallic Fe to the loop system. The corrosion rates calculated above indicate that the amounts of Fe, if completely deposited at the loop surfaces where the FeF<sub>2</sub>-Cr reaction occurred, would amount at most to 10<sup>-3</sup> g/cm<sup>2</sup>. This value corresponds to a uniform Fe deposit of 1.27 microns. Since no evidence of a metal layer could be discerned metallographically, it is presumed that diffusion of Fe into the base metal occurred simultaneously with the leaching of Cr from the metal.

In summary, the depletion rates of Cr in the  $\text{FeF}_2$  experiment followed closely the pattern predicted by the assumption that corrosion rates were controlled by the solid-state diffusion rates of Cr in INOR-8. In addition, the observed diffusion rates corresponded closely to the diffusion rate of tracer determined under non-corrosive conditions in Loop 1248.

#### Corrosion of INOR-8 by $\text{UF}_4$

The diffusivity data obtained through the operation of Loops 1248 and 1249 can be applied to calculations of the corrosion rates of INOR-8 by fluoride mixtures containing  $\text{UF}_4$ . These calculations, however, are considerably more complex than in the case of the  $\text{FeF}_2$  corrosion experiment.

Cr mass transfer by  $\text{UF}_4$ -containing salts. If pure salt containing  $\text{UF}_4$  but no corrosion products were added to an INOR-8 loop operating polythermally, all points of the loop initially would experience a loss of Cr in accordance with the Cr- $\text{UF}_4$  reactions (equations 7 and 12) discussed in Chapter III. Eventually the corrosion-product concentration of the circulating salt would increase as a result of this reaction to an amount corresponding to equilibrium at the lowest temperature in the loop. At regions of higher temperature, however, a driving force would still exist for Cr

to react with  $\text{UF}_4$ . Thus, the corrosion-product concentration would continue to increase, and the temperature points at equilibrium would begin to move away from the coldest temperature point. At this stage, Cr would be returned to the walls of the coldest point of the system. The rise in corrosion-product concentration in the circulating salt would continue until the amount of Cr returning to the walls exactly balanced the amount of Cr entering the system in the hot-leg regions. Under these conditions, the two positions of the loop at equilibrium with the salt, which are termed the "balance points," would not shift measurably with time. In addition, the rate of the movement or mass transport of Cr from hot- to cold-leg regions would gradually diminish with time if this rate were diffusion controlled.

During the initial or unsteady-state period of corrosion, the mathematical interpretation of Cr migration rates in polythermal systems is extremely complex, because of rapid compositional changes which occur continuously in both the salt mixture and at the surface of the container wall. A manifestation of this complexity is apparent in cold-leg regions, where Cr concentration gradients are reversed as corrosion products build up within the salt. Unfortunately, the effects of unsteady-state operation serve also to complicate the interpretation of steady-state operation. However, an idealized approach to the study of Cr migration under

steady-state conditions is afforded by assuming the salt mixture to be pre-equilibrated so as to contain amounts of  $\text{CrF}_2$  and  $\text{UF}_3$  which establish a steady-state condition at the beginning of loop operation.\*

Calculation of corrosion rates. Calculations for the case of pre-equilibrated salt systems were developed by Evans<sup>29</sup> in conjunction with corrosion studies of Inconel and can be extended also to INOR-8. As a means for demonstrating these calculations, it is convenient to apply them to a pre-equilibrated polythermal INOR-8 loop in which the salt system  $\text{NaF-ZrF}_4-\text{UF}_4$  (50-46-4 mole per cent) is circulated between the temperature limits of 600°C and 800°C. It is assumed that the steady-state salt concentration is in equilibrium with INOR-8 at the coldest point of the system, i.e., that the balance point of the system is at 600°C. Under this condition, the amount of Cr depletion and hence the corrosion rate at 800°C is the highest attainable under steady-state

---

\*It is evident that pre-equilibration of the salt mixture would afford an expedient means for reducing corrosive attack in INOR-8 systems, since it would eliminate the initial or unsteady-state period of corrosion during which relatively high corrosion rates are sustained. However, to achieve criticality in reactor systems which are presently under study, it is planned to add  $\text{UF}_4$  incrementally to the salt mixture until a desired reactivity is achieved. Under these conditions, the program required to maintain a pre-equilibrated salt with each  $\text{UF}_4$  level becomes extremely complex.

conditions.\* Additional assumed boundary conditions are:

1. The overall rate of transfer is controlled by the diffusion rate of Cr in the container material, since this diffusion rate can be shown to be considerably lower than the rates of reaction and of mixing which are involved in the transfer process.

2. Chemical equilibrium with respect to Cr and the salt mixture exists at every surface point within the loop system.

3. At any time the cumulative amount of Cr removed from the hot zone equals the cumulative amount deposited in the cold zone. Accordingly, the concentrations of  $\text{UF}_3$ ,  $\text{UF}_4$ , and  $\text{CrF}_2$ , assuming the salt to be rapidly circulated, do not vary with loop position or time.

In accordance with condition (2), the surface concentration,  $(\underline{\text{N}}_{\text{Cr}})_s$ , at the  $800^{\circ}\text{C}$  temperature point can be expressed in terms of the equilibrium constant,  $K_a$ , determined for equation 7 in Chapter III.

$$K_a = \frac{a_{\text{UF}_3}^2 \cdot a_{\text{CrF}_2}}{a_{\text{UF}_4}^2 \cdot (\underline{\text{N}}_{\text{Cr}})_s} \approx \frac{a_{\text{UF}_3}^2 \cdot a_{\text{CrF}_2}}{a_{\text{UF}_4}^2 \cdot (\underline{\text{N}}_{\text{Cr}})_s} \quad (24)$$

\*This condition in the case of the  $\text{NaF-ZrF}_4-\text{UF}_4$  salt system would be attainable only if the loop surface area and hence the rate of Cr deposition at  $600^{\circ}\text{C}$  is infinite with respect to the surface area and rate of Cr removal at higher temperature points.

$$[(\underline{N}_{Cr})_s]_{800^\circ C} = \frac{1}{(K_a)_{800^\circ C}} \left[ \frac{a_{UF_3}^2 \cdot a_{CrF_2}}{a_{UF_4}^2} \right] \quad (25)$$

but

$$\frac{a_{UF_3}^2 \cdot a_{CrF_2}}{a_{UF_4}^2} = [(\underline{N}_{Cr})_s]_{600^\circ C} \cdot (K_a)_{600^\circ C} \quad (26)$$

so that

$$[(\underline{N}_{Cr})_s]_{800^\circ C} = \frac{(K_a)_{600^\circ C}}{(K_a)_{800^\circ C}} [(\underline{N}_{Cr})_s]_{600^\circ C} \quad (27)$$

The balance points of the system, which are at  $600^\circ C$ , have been defined such that

$$[(\underline{N}_{Cr})_s]_{600^\circ C} \simeq (\underline{N}_{Cr})_{INOR-8} \quad (28)$$

Therefore

$$(\underline{N}_{Cr})_s|_{800^\circ C} = \frac{(K_a)_{600^\circ C}}{(K_a)_{800^\circ C}} (\underline{N}_{Cr})_{INOR-8} \quad (29)$$

and

$$\frac{(C_s)_{800^\circ C}}{C_o} = \frac{(K_a)_{600^\circ C}}{(K_a)_{800^\circ C}} \quad (30)$$

where

$C_s$  = surface concentration of Cr ( $g/cm^3$ )

$C_o$  = original Cr concentration of INOR-8 ( $g/cm^3$ )

The equilibrium constants for the reference salt system at  $600^\circ C$  and  $800^\circ C$  have been measured to be  $3.2 \times 10^{-4}$  and

$5.9 \times 10^{-4}$ , respectively<sup>30</sup>; accordingly,

$$(C_s)_{800^{\circ}C} = \left(\frac{3.2}{5.9}\right) C_o = 0.54 C_o \quad (31)$$

Boundary condition (1) states that the overall Cr migration rate can be expressed in terms of the diffusional flow which takes place in the metal. The applicable diffusion equation for the  $800^{\circ}C$  temperature position under the boundary condition of constant surface concentration is given as

$$C(x,t) = C_s - \Delta C \operatorname{erf} \frac{x}{2\sqrt{Dt}} \quad (32)$$

where

$C(x,t)$  = Cr concentration at depth  $x$  after time  $t$

$$\Delta C = C_s - C_o$$

Substituting the value for  $C_s$  given by equation 31 in equation 32, it follows that

$$\frac{C(x,t)}{C_o} = 0.54 + 0.46 \operatorname{erf} \frac{x}{2\sqrt{Dt}} \quad (33)$$

Knowing the concentration gradient of Cr, it is possible to calculate the total amount of Cr,  $\Delta M$ , which has been removed from a unit area of surface during time  $t$ , as follows:

$$\Delta M = \int_0^\infty [C_o - C(x,t)] dx = 0.46 C_o \int_0^\infty (1 - \operatorname{erf} \frac{x}{2\sqrt{Dt}}) dx$$

$$\Delta M = 0.46 \left( \frac{2}{\sqrt{\pi}} C_o \sqrt{Dt} \right) \quad (34)$$

Accordingly, the rate of removal of Cr (per unit of area) at any time  $t$  is given as

$$\frac{d(\Delta M)}{dt} = 0.46 \left( \frac{1}{\sqrt{\pi}} c_0 \sqrt{D \frac{1}{t}} \right) = \frac{\Delta M}{2t} \quad (35)$$

Values of the corrosion rate and total attack at 800°C predicted by equations 32 and 33, respectively, are plotted in Figure 24 for time periods up to 18 months. The corrosion rate, measured in units of  $10^{-4}$  g/mo $\cdot$ cm $^2$ , is seen to decline to a relatively low value after the first 3 months of operation. After 18 months the specimen loses only about 1 mg/cm $^2$  of Cr. At this time the midpoint of Cr depletion\* is located at a distance of only 0.0013 in. from the exposed surface.

The following conclusions can be drawn from calculations of the corrosion of INOR-8 under the assumed steady-state conditions:

1. Even under the assumption that corrosion products remained at a level in equilibrium with the INOR-8 container at its coldest point (600°C), the Cr surface concentration at 800°C is lowered to no more than one-half of the original surface concentration, as given by equation 31. Thus at no point in any steady-state system operating between 600°C and 800°C with the postulated salt mixture would the Cr concentration of the container system fall below 3.5 per cent.

---

\*The "midpoint of depletion" as applied to diffusion processes refers to the point in a semi-infinite medium which has reached a concentration midway between the initial and ultimate concentration. Its distance from the surface is approximately equal to  $\sqrt{Dt}$ .

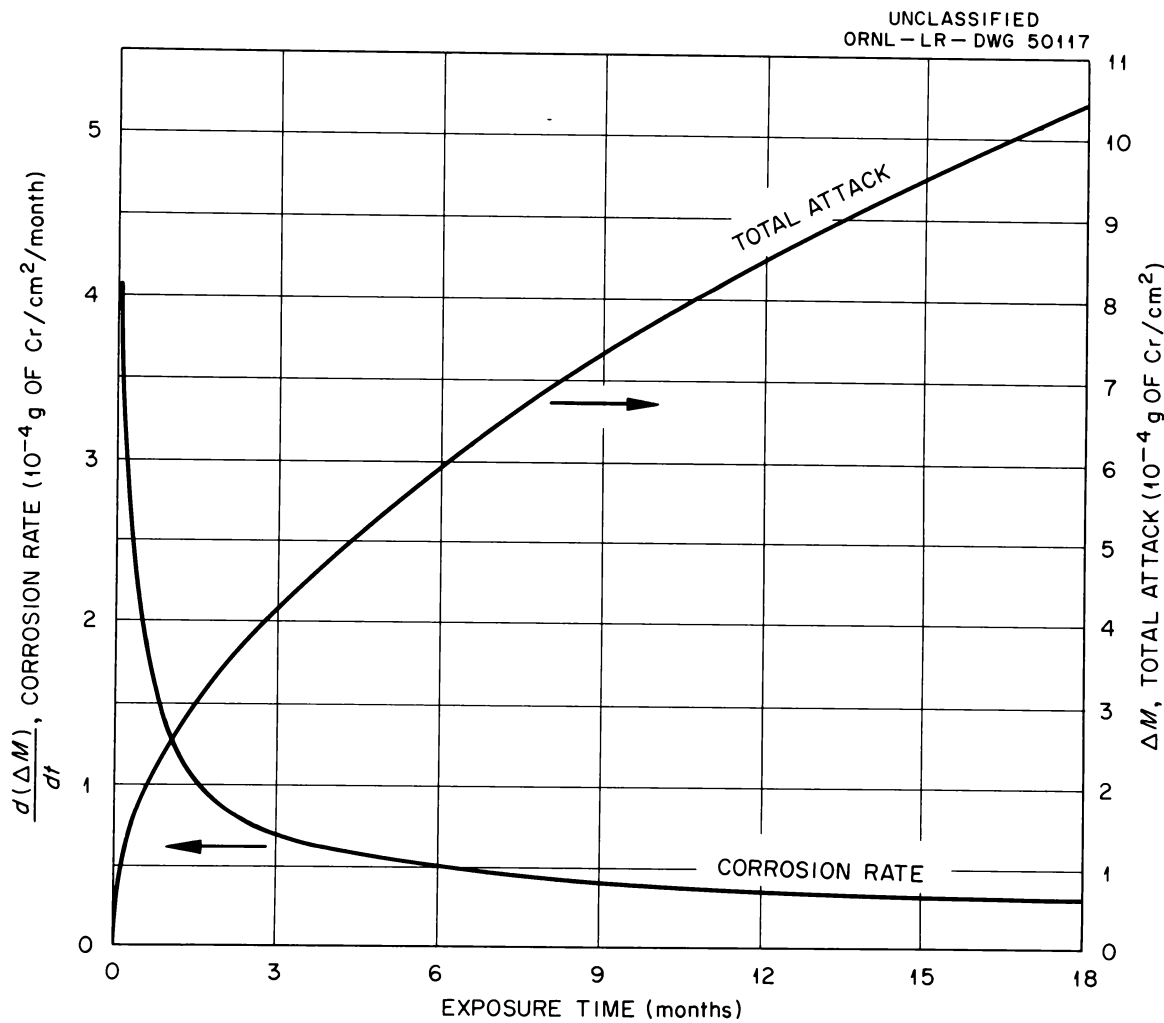


Figure 24. Calculated corrosion rate and cumulative attack for 800°C section of INOR-8 loop containing pre-equilibrated NaF-ZrF<sub>4</sub>-UF<sub>4</sub> (50-46-4 mole per cent) salt. Assumed test conditions: hot-leg temperature - 800°C; cold-leg temperature - 600°C; salt in equilibrium with INOR-8 at 600°C.

2. Under the assumption that  $N_{Cr} \approx a_{Cr}$ , the rate of Cr depletion is in direct proportion to the Cr concentration of the container material (equation 33). Therefore, the reduction of Cr mass transfer which is effected by modifying the Cr concentration of the container material is in direct proportion to the resultant reduction in the thermodynamic activity of the Cr constituent.

## CHAPTER VI

### CONCLUSIONS AND RECOMMENDATIONS

#### I. CONCLUSIONS

1. The corrosion properties of solid-solution alloying elements in the Ni-17 per cent Mo system were investigated in molten mixtures of NaF-LiF-KF-UF<sub>4</sub> (11.2-41.0-45.3-2.5 mole per cent). The corrosion susceptibility of alloying additions was found to increase in the following order: Fe, Nb, V, Cr, W, Ti, and Al. With the exception of W, the susceptibility of these elements to corrosion increased in approximately the same order as the stabilities of fluoride compounds of the elements.

2. The corrosion-product concentrations produced by either Fe, Nb, or W alloying additions in the above salt mixture were much lower when these elements existed in combination with Cr, Ti, or Al than when they existed as single alloying additions. In contrast, corrosion-product concentrations associated with Cr, Ti, or Al were unchanged by the presence of other alloying constituents.

3. Corrosive attack in Ni-Mo alloys containing single alloying additions was manifested by the formation of small surface pits. The depth of pitting was in the range of 0.001 to 0.002 in. after both 500-hr and 1000-hr test intervals.

Subsurface voids to depths up to 0.004 in. were also detected in alloys containing Al in amounts greater than 2 atomic per cent.

4. Alloys containing multiple additions were in all cases attacked to greater depths than alloys containing single alloying additions. The highest depths of attack which ranged from 0.003 to 0.0045 in. in 1000 hours were incurred in alloys containing combined additions of Al and Cr or Al and Ti.

5. The diffusivities of Cr-51 in INOR-8 were measured between temperatures of 680°C and 870°C and found to be in the range  $10^{-12}$  to  $10^{-14}$  cm<sup>2</sup>/sec. These values were similar to diffusivities which have been reported for the diffusion of Cr in Ni-Cr alloys. Diffusivities of Cr in INOR-8 in which Cr concentration had been depleted by exposure to FeF<sub>2</sub> were similar to Cr diffusivities determined under conditions of constant Cr concentration.

6. Diffusivities which governed the rate of Cr-51 movement in areas of the INOR-8 alloy farthest removed from the Cr-51 source were higher than diffusivities which governed movement in the alloy closer to the source. This observation was attributed to the increased importance of grain-boundary diffusion relative to volume diffusion at higher penetration depths.

7. The mechanisms which control the corrosion behavior of INOR-8 in fluoride salt mixtures may be investigated by

implanting Cr-51 in a thermal convection loop and following the movement of this tracer under controlled corrosion conditions. In an experiment of this type, which was conducted with the corrosive agent  $\text{FeF}_2$ , the observed corrosion rates corresponded to those predicted by assuming corrosion to be controlled by the diffusion rates of Cr in INOR-8.

8. The corrosion rates of INOR-8 in fluoride mixtures containing  $\text{UF}_4$  may be calculated under the assumptions that these rates are controlled by the diffusion rates of Cr in INOR-8 and that the surface concentration of Cr at the container surface is in equilibrium with the salt mixture. Such calculations indicate that the Cr concentration of INOR-8 loops which contain pre-equilibrated mixtures of  $\text{NaF-ZrF}_4-\text{UF}_4$  (50-46-4 mole per cent) between 600°C and 800°C should remain at all times above 3.5 per cent.

## II. RECOMMENDATIONS

1. The results of experiments carried out in recent years on the mass transport of Cr in INOR-8 systems containing fluoride fuels have strongly suggested that the over-all mass transport rate is controlled by the diffusion rate of Cr within the metal. The present studies provide a basis for the controlled implantation of radioactive Cr within the walls of any INOR-8 loop system, so that the movement of Cr may be followed in terms of the migration of tracer. It is,

therefore, recommended that a  $\text{UF}_4$  corrosion experiment be programmed such that the observed movement of radiotracer can be correlated with computations of mass transport rates based on measured diffusion rates of Cr in INOR-8.

2. As an adjunct to predictions of the corrosion behavior of INOR-8 in  $\text{UF}_4$ -containing salts, the thermodynamic activity of Cr in Ni-Mo systems should be determined for Cr concentrations in the range from 3 to 10 per cent.

3. Experimental procedures which were utilized in the present investigation to determine Cr diffusivities in INOR-8 could be extended without modification to evaluations of Cr diffusivities in any alloy system composed of Fe, Cr, Mo, and Ni. It would be of interest to apply this technique to evaluations of diffusion coefficients of Cr in Fe-base alloys and to compare rates in these systems with rates which have been determined for Ni-base alloys.

**LIST OF REFERENCES**

## LIST OF REFERENCES

1. Briant, R. C., and A. M. Weinberg, "Molten Fluorides as Power Reactor Fuels," Nuclear Science and Eng. 2, 797-803 (1957).
2. Bettis, E. S., et al., "The Aircraft Reactor Experiment - Design and Construction," Nuclear Science and Eng. 2, 804-825 (1957).
3. Manly, W. D., et al., Aircraft Reactor Experiment - Metallurgical Aspects, ORNL-2349 (1957).
4. Manly, W. D., et al., "Metallurgical Problems in Molten Fluoride Systems," Progr. in Nuclear Energy, Ser. IV 2, 164 (1960).
5. Redman, J. D., ORNL-2440, Classified, pp. 78-82 (1957).
6. Ibid., p. 78.
7. Ibid., p. 79.
8. Evans, R. B., ORNL-2440, Classified, pp. 104-113 (1957).
9. Clausing, R. E., P. Patriarca, and W. D. Manly, Aging Characteristics of Hastelloy B, ORNL-2314 (1957).
10. Inouye, H., Private Communication.
11. Stoffel, D. W., and E. E. Stansbury, "A Metallographic and X-ray Study of Ni Alloys of 20-30 Per Cent Mo," Report No. 1 under Subcontract No. 582 under Contract No. W-7405 eng-26, Knoxville, Tenn., Dept. of Chem. Eng. of the Univ. of Tenn. (1955).
12. Evans, R. B., op. cit., pp. 100-104.
13. Sturm, B. J., "Preparation of Pure Fluoride Compounds," MSRP Quarterly Progress Report, ORNL-2626, p. 107 (1958).
14. Evans, R. B., J. H. DeVan, and G. M. Watson, Self-Diffusion of Chromium in Nickel-Based Alloys, ORNL-2982 (in press).
15. DeVan, J. H., An Evaluation of Electro-Machining for the Analysis of Metal Surfaces, ORNL-CF-59-6-109 (1959).

16. Churchill, R. V. Modern Operational Mathematics in Engineering. Second edition, pp. 128-143. New York: McGraw-Hill Book Company, Inc., 1958.
17. Adamson, G. M., R. S. Crouse, and W. D. Manly, Interim Report on Corrosion by Alkali-Metal Fluorides: Work to May 1, 1953, ORNL-2337 (1959).
18. Redman, J. D., op. cit., p. 79.
19. Grimes, W. R., ORNL-2106, Classified, pp. 96-99 (1956).
20. Richardson, L. S., D. C. Vreeland, and W. D. Manly, ORNL-1491, Classified, pp. 15-19 (1953).
21. Glassner, A., The Thermodynamic Properties of the Oxides, Fluorides, and Chlorides to 2500°K, ANL-5750.
22. Inouye, H., Private Communication.
23. Evans, R. B., J. H. DeVan, and G. M. Watson, op. cit.
24. Ibid.
25. Gruzin, P. L., and G. B. Federov, Doklady Akad. Nauk S.S.R., 105, 264-67 (1955).
26. Fisher, J. S., "Calculation of Diffusion Penetration Curves for Surface and Grain Boundary Diffusion," J. Appl. Phys., 22, 74 (1951).
27. Whipple, R. T. P., "Concentration Contours in Grain Boundary Diffusion," Phil. Mag., 45, 1225 (1954).
28. Evans, R. B., J. H. DeVan, and G. M. Watson, op. cit.
29. Evans, R. B., op. cit., pp. 104-113.
30. Redman, J. D., op. cit., p. 79.

## **APPENDICES**

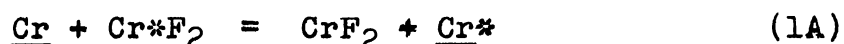
## APPENDIX A

## Cr DIFFUSION MEASUREMENTS

As discussed in Chapter III, values of the diffusion coefficients for Cr in Ni-base alloys are pertinent to the interpretation of selective corrosive attack which occurs in these alloys when exposed to flowing fluoride salts. Toward this end, methods were developed at ORNL for the application of the radiotracer Cr-51 to the study of Cr diffusion in Ni and Ni-Mo alloys.<sup>1</sup> The objective of these studies was to determine the rate of movement of Cr into or out of the alloy as a function of surface concentration, time, and temperature. Accordingly, the coefficients computed represent the combined effects of grain-boundary and matrix diffusion, and no rigorous attempt was made to separate the relative contributions of either process.

I. APPLICATION OF FUSED FLUORIDE  
MIXTURES TO DIFFUSION STUDIES

The experimental methods employed for the diffusion studies utilized the radioisotope Cr-51, which was placed on the surface of the selected diffusion medium through the following exchange reaction:



where Cr\* refers to the "tagged" atom, Cr-51

The  $\text{Cr}^*\text{F}_2$  was dissolved in a carrier salt composed of  $\text{NaF-ZrF}_4$  (53-47 mole per cent), which was kept in contact with the alloy throughout the diffusion experiments. In addition to supplying the metal surface with tracer, this salt mixture also served to keep surfaces of the alloy free from contamination.

Chemical reactions occurring between the  $\text{NaF-ZrF}_4$  salt mixture and alloy systems under study had been shown experimentally, as well as from free energy considerations, to be extremely limited.<sup>2</sup> It was reasonable to assume, therefore, that the only reaction resulting at the surface was the exchange reaction, equation 1A. If, in addition, it was assumed that radioactive Cr ( $\text{Cr}^*$ ) was uniformly distributed throughout the system in the same relative proportions as natural Cr, the concentration of  $\text{Cr}^*$  at the surface of the alloy at any temperature was given by

$$\frac{\frac{N_{\text{Cr}^*}}{N_{\text{Cr}}}}{\frac{N_{\text{CrF}_2}}{N_{\text{Cr}}}} = \frac{\frac{N_{\text{Cr}^*\text{F}_2}}{N_{\text{CrF}_2}}}{\frac{N_{\text{Cr}^{++}}}{N_{\text{Cr}^{++}}}} \quad (2A)$$

or

$$\frac{\frac{w_{\text{Cr}^*}}{w_{\text{Cr}}}}{\frac{w_{\text{Cr}^{++}}}{w_{\text{Cr}^{++}}}} = \frac{\frac{w_{\text{Cr}^*\text{F}_2}}{w_{\text{CrF}_2}}}{\frac{w_{\text{Cr}^{++}}}{w_{\text{Cr}^{++}}}} \quad (3A)$$

where W refers to weight fraction

Thus, the concentration of tracer atoms at the surface of the test specimens was established by the ratio of the radioactive

to non-radioactive ions in the  $(Cr, Cr^*)F_2$  addition, and not by the total amount of the addition.

## II. DIFFUSION EQUATIONS

In accordance with Fick's second law, which is fundamental to diffusion theory, the flow of Cr-51 can be expressed as

$$\frac{\partial C_{Cr^*}}{\partial t} = DA \frac{\partial^2 C_{Cr^*}}{\partial x^2} \quad (4A)$$

where

$C_{Cr^*}$  = concentration of  $Cr^*$

A = area through which diffusion occurs,  $cm^2$

D = diffusion coefficient,  $cm^2/sec$

x = distance from the surface of the diffusion medium, cm

With the constant concentration of the  $Cr^*F_2$  in the molten salt during a given exposure period, alloy specimens immersed in the salt absorbed "tagged" Cr under conditions of constant surface potential. That is, the concentration of  $Cr^*$  at the surface remained constant with time. Furthermore, the thickness of the loop wall could be regarded as infinite relative to the depth of tracer penetration. Under these boundary conditions, equation 3A has the following solution in terms of depth x and time t:

$$C_{Cr^*}(x, t) = (C_{Cr^*})_{x=0} erfc \frac{x}{2\sqrt{Dt}} \quad (5A)$$

Accordingly, the total amount of radiotracer which has entered the diffusion medium after time  $t$  may be calculated to be

$$\Delta M = A \int_0^\infty C_{Cr^{**}}(x, t) dx = \frac{2}{\sqrt{\pi}} A \sqrt{Dt} (C_{Cr^{**}})_{x=0}$$

but

$$(C_{Cr^{**}})_{x=0} = (\rho w_{Cr^{**}})_{x=0} = \rho w_{Cr} \frac{w_{Cr^{++*}}}{w_{Cr^{++}}} \quad (6A)$$

so

$$\frac{\Delta M}{w_{Cr^{++*}}} = \frac{y}{z} = \frac{2}{\sqrt{\pi}} A \rho \frac{w_{Cr}}{w_{Cr^{++}}} \sqrt{Dt} \quad (7A)$$

where

$\rho$  = density of the alloy

$y$  = total counts of the entire specimen per min

$z$  = counts of the salt per gm per min at  $t$

The variable  $y$  is a measure of the total amount of tracer gained by the specimen;  $z$  is an indirect measure of the tracer concentration which is maintained on the specimen surface during exposure to the salt.

After constant-potential exposure, self-diffusion coefficients were determined by measuring the tracer concentration profile through successive removal and analysis of thin layers of alloy. An electropolishing technique was developed for achieving closely controlled surface removal.<sup>3</sup> The electropolishing experiments were conducted as follows:

after salt exposure, the specimens were alternately counted and polished until less than 10 per cent of the original activity remained in the alloy. The per cent of activity remaining after each polishing was plotted as a function of the cumulative penetration distances (wall thickness minus the sum of polishing increments). The experimental plot was compared to a generalized plot of an equation applicable to the experimental procedure. For a constant-potential, semi-infinite system, with an initial tracer concentration of zero, the equation is

$$F(x) = 100\sqrt{\pi} \int_x^{\infty} \operatorname{erfc} u du \quad (8A)$$

where

$F(x)$  = per cent of original activity remaining at penetration  $x$ , cm

$$u = \frac{x}{2(Dt)^{\frac{1}{2}}}$$

Values of  $\int_x^{\infty} \operatorname{erfc} u du$  are available in tabular form in the literature.<sup>4</sup>

### III. TEST APPARATUS

Diffusion experiments utilizing fused fluoride salts as the tracer carrier may be conveniently conducted in either a static capsule or flowing loop system. A detailed description of the procedures utilized to perform capsule experiments has been given by Evans, et al.<sup>5</sup> Briefly, the alloy specimens

employed were small (1/4-in OD thermocouple wells) and were immersed in a relatively large volume of salt (200 cc). The salt was contained in a vessel of the same alloy material which, prior to the introduction of the sample, had been heated in contact with the solution to about 950°C and had absorbed Cr<sup>6+</sup> for some time. After this pretreatment, the temperature of the system was lowered to the temperature of interest and the specimens were introduced. In this manner, not only the salt but also the walls of the vessel served as reservoirs of Cr<sup>6+</sup>. Experimentally, the Cr<sup>6+</sup>F<sub>2</sub> concentration in the solution could be maintained essentially constant throughout the duration of the specimen exposure.

Loop experiments offer several advantages over the capsule experiments. It is possible in a loop experiment to effect a gradient of temperatures, so that a single test run can provide diffusion coefficients for a multiplicity of temperature levels. Furthermore, in loop experiments all of the alloy specimens are exposed to the same salt solution, resulting in better control of the salt radioactivity as an experimental variable.

The thermal convection harp, described in Chapter IV, affords a simple and economical means for achieving the desired temperature gradient and dynamic flow conditions. Salt containing Cr<sup>6+</sup>F<sub>2</sub> is introduced into the loop in the same manner as in capsule experiments. To afford a constant Cr

activity at the surface, however, additions of Cr\*F<sub>2</sub> during the course of the experiment may be required to replace Cr-51 which has transferred from the salt to the metal. After operation with salt, several small sections are taken from around the loop which effectively provide a series of capsule tests at various temperature levels. Each of these sections is counted for total radioactivity, as in the case of capsule experiments, and then the inside surfaces are polished to obtain the Cr-51 concentration profile.

**APPENDIX B****DATA FOR RADIOTRACER EXPERIMENTS**

Values of Cr diffusivities and data utilized for their computation are presented in this section.

Table XV lists the surface area, density, and Cr contents of the INOR-8 test specimens removed from radiotracer Loops 1248 and 1249. Also shown are the Cr concentrations and radioactivity levels of the salt mixtures circulated in these loops.

Tables XVI and XVII provide tabulations of Cr diffusivities, along with data used for their determination, based on total specimen radioactivity. Data for Loop 1248 are shown in Table XVI and those for Loop 1249, in Table XVII.

The procedures which were followed in the calculation of Cr diffusivities based on the Cr-51 concentration gradients of specimens from Loops 1248 and 1249 are indicated in Tables XVIII and XIX, respectively. The values of Cr diffusivities obtained by this method for Loops 1248 and 1249 are listed in Tables XX and XXI.

TABLE XV

PROPERTIES OF INOR-8 SPECIMENS AND SALT MIXTURES  
USED FOR RADIOTRACER LOOP EXPERIMENTS

<u>Property</u>	<u>Symbol*</u>	<u>Experimental Value</u>	
		<u>Loop 1248</u>	<u>Loop 1249</u>
Surface Area of Test Specimens ( $\text{cm}^2$ )	A	11.039	11.039
Density of Test Specimens ( $\text{g}/\text{cm}^3$ )	$\rho$	8.79	8.79
Weight Fraction of Cr in Test Specimens	$w_{\text{Cr}}$	0.0690	0.0741
Weight Fraction of $\text{Cr}^{++}$ in Salt	$w_{\text{Cr}^{++}}$	0.00180	0.00277
Radioactivity Level of Salt (counts for 2-min counting period)**	z	681,820	307,000

\*Symbol refers to the property designation used in equation 7A.

\*\*Correction for radioactive decay was provided by recording salt radioactivity and specimen radioactivity at the same point in time.

TABLE XVI  
TOTAL SPECIMEN RADIOACTIVITIES AND CORRESPONDING Cr DIFFUSIVITIES  
MEASURED IN INOR-8 LOOP 1248 AFTER 500-HR EXPOSURE TO SALT

Spec. No.	Operating Temp. (°C)	Thermal Coefficient of Expansion between 20°C and Operating Temp.*	Total Specimen Radioactivity** [(counts/2min)x10 <sup>-3</sup> ]	D x 10 <sup>13</sup> (cm <sup>2</sup> /sec)	Log <sub>10</sub> D
1	832	1.012	1,807	2.72	-12.566
2	870	1.012	2,278	4.33	-12.364
3	867	1.012	2,207	4.07	-12.390
4	821	1.012	1,664	2.31	-12.638
5	849	1.012	1,997	3.33	-12.478
6	826	1.012	1,595	2.49	-12.604
7	801	1.011	1,532	1.95	-12.710
8	786	1.011	1,385	1.60	-12.798
9	765	1.010	1,212	1.22	-12.915
10	691	1.009	689	0.394	-13.405
11	700	1.009	760	0.479	-13.320
12	716	1.010	858	0.616	-13.210
13	728	1.010	911	0.695	-13.158
14	746	1.010	988	0.812	-13.091
15	807	1.011	1,629	2.20	-12.658

\*This factor was used to correct for changes in density and surface area occurring between room temperature, where measurements of these properties were made, and the specimen operating temperatures.

\*\*Radioactivity of specimens was determined at the same time that salt radioactivity (Table XV) was recorded.

TABLE XVII  
TOTAL SPECIMEN RADIOACTIVITIES AND CORRESPONDING Cr DIFFUSIVITIES  
MEASURED IN INOR-8 LOOP 1249

Spec. No.	Operating Temp. (°C)	Thermal Coefficient of Expansion between 20°C and Operating Temp.*	Total Specimen Radioactivity** [(counts/2min)×10 <sup>-3</sup> ]	D × 10 <sup>13</sup> (cm <sup>2</sup> /sec)	Log <sub>10</sub> D
1	813	1.011	402.8	2.48	-12.606
2	836	1.012	467.6	3.35	-12.475
3	857	1.012	477.8	3.50	-12.456
4	852	1.012	462.7	3.28	-12.484
5	844	1.012	478.2	3.50	-12.456
6	828	1.012	426.6	2.78	-12.556
7	810	1.011	435.1	2.89	-12.539
8	810	1.011	402.3	2.48	-12.606
9	804	1.011	391.4	2.34	-12.631
10	684	1.009	129.2	0.254	-13.595
11	694	1.009	127.6	0.249	-13.604
12	718	1.010	160.3	0.391	-13.408
13	742	1.010	181.3	0.502	-13.299
14	768	1.011	242.9	0.902	-13.044
15	813	1.011	430.9	2.84	-12.546

\*This factor was used to correct for changes in density and surface area occurring between room temperature, where measurements of these properties were made, and the specimen operating temperatures.

\*\*Radioactivity of specimens was determined at the same time that salt radioactivity (Table XV) was recorded.

TABLE XVIII

SAMPLE CALCULATIONS OF Cr DIFFUSIVITIES BASED ON CONCENTRATION GRADIENT  
OF Cr-51 IN SPECIMENS FROM LOOP 1248

Specimen No. 15 (exposed at 807°C)  
Time of Exposure =  $1.80 \times 10^6$  sec

<u>x (microns removed from surface)*</u>	<u>Radioactivity of Specimen (counts/2min)</u>	<u>F(x) (per cent of Cr-51 left in specimen)</u>	<u>u** (<math>\frac{x}{2\sqrt{Dt}}</math>)</u>	<u><math>2\sqrt{Dt}</math> (microns)</u>	<u><math>D \times 10^{13}</math> (<math>\text{cm}^2/\text{sec}</math>)</u>	<u><math>D \times 10^{13}</math> (<math>\text{cm}^2/\text{sec}</math>) Corrected***</u>
0.00	783,540	100.0				
0.83	-	90.0	0.055	15.1	3.16	3.23
1.08	673,700	86.0				
2.15	573,880	73.2				
2.40	-	70.0	0.19	12.6	2.21	2.26
4.30	397,390	50.7				
4.30	-	50.0	0.35	12.3	2.10	2.15
6.45	272,190	34.7				
7.52	-	30.0	0.57	12.7	2.24	2.29
10.8	130,130	16.6				
15.1	65,100	8.31				
Average = 2.60						

\*Values of x corresponding to  $F(x) = 90, 70, 50$ , and  $30$  per cent were interpolated from experimental data.

\*\*Values of u represent solutions of equation 8A (Appendix A).

\*\*\*Correction takes into account thermal contraction; see Note (\*), Table XVI.

TABLE XIX

SAMPLE CALCULATIONS OF Cr DIFFUSIVITIES BASED ON CONCENTRATION GRADIENT  
OF Cr-51 IN SPECIMENS FROM LOOP 1249

Specimen No. 15 (exposed at 813°C)  
Total Time of Exposure to Salt ( $t'$ ) =  $3.78 \times 10^6$  sec

<u>x (microns removed from surface)*</u>	<u>Radioactivity of Specimen (counts/2min)</u>	<u>F(x) (per cent of Cr-51 left in specimen)</u>	<u>w** (<math>\frac{x}{2\sqrt{Dt}}</math>)</u>	<u><math>2\sqrt{Dt}</math> (microns)</u>	<u><math>D \times 10^{13}</math> (cm<sup>2</sup>/sec)</u>	<u><math>D \times 10^{13}</math> Corrected*** (cm<sup>2</sup>/sec)</u>
0.00	324,567	100.0				
0.49	323,947	99.8				
0.99	323,067	99.5				
1.48	322,937	99.4				
2.47	318,027	98.0				
3.46	312,697	96.3				
5.75	-	90.0	0.225	25.6	4.33	4.42
5.79	289,917	89.3				
8.40	261,517	80.5				
11.4	-	70.0	0.430	26.5	4.64	4.74
13.3	205,557	63.3				
17.4	-	50.0	0.604	28.8	5.48	5.60
18.3	152,467	47.0				
24.6	-	30.0	0.817	30.1	5.99	6.12
25.7	89,307	27.5				
33.1	48,427	14.9				
38.0	31,527	9.7			Average = 5.22	

\*Values of x corresponding to  $F(x) = 90, 70, 50$ , and  $30$  per cent were interpolated from experimental data.

\*\*Values of w represent solutions to equation 16 (Chapter IV).

\*\*\*Correction takes into account thermal contraction; see Note (\*), Table XVI.

TABLE XX  
Cr DIFFUSIVITIES MEASURED IN INOR-8 LOOP 1248  
BASED ON Cr-51 CONCENTRATION PROFILE

Specimen No.	Diffusivities Calculated From Concentration Gradient Based on Radioactivity Entering Electrolyte			Diffusivities Calculated From Concentration Gradient Based on Radioactivity Remaining in Specimen		
	$D \times 10^{13}$ ( $\text{cm}^2/\text{sec}$ )	$\log_{10} D$	$D \times 10^{13}$ ( $\text{cm}^2/\text{sec}$ )	$\log_{10} D$		
1	5.67	-12.246	-	-	-	
2	13.1	-11.883	-	-	-	
3	9.75	-12.011	9.17	-12.038		
4	4.81	-12.318	4.11	-12.386		
5	8.07	-12.093	6.27	-12.202		
6	5.17	-12.286	4.16	-12.381		
7	2.94	-12.532	2.82	-12.550		
8	2.78	-12.556	2.51	-12.600		
9	1.62	-12.790	1.65	-12.782		
10	0.253	-13.596	0.256	-13.592		
11	-	-	0.253	-13.596		
12	0.253	-13.596	0.316	-13.500		
13	-	-	0.328	-13.484		
14	-	-	0.518	-13.286		
15	2.58	-12.588	2.43	-12.614		

TABLE XXI  
Cr DIFFUSIVITIES MEASURED IN INOR-8 LOOP 1249  
BASED ON Cr-51 CONCENTRATION PROFILE

Specimen No.	Diffusivities Calculated From Concentration Gradient Based on Radioactivity Entering Electrolyte		Diffusivities Calculated From Concentration Gradient Based on Radioactivity Remaining in Specimen	
	$D \times 10^{13}$ $(\text{cm}^2/\text{sec})$	$\log_{10} D$	$D \times 10^{13}$ $(\text{cm}^2/\text{sec})$	$\log_{10} D$
1	6.59	-12.181	6.13	-12.212
2	9.54	-12.020	8.87	-12.052
3	16.5	-11.787	16.1	-11.793
4	9.95	-12.002	9.14	-12.039
5	12.7	-11.896	12.1	-11.917
6	9.54	-12.021	8.66	-12.063
7	5.67	-12.246	4.98	-12.302
8	4.74	-12.324	3.83	-12.416
9	3.66	-12.436	3.28	-12.484
10	0.435	-13.362	0.382	-13.418
11	0.571	-13.244	0.511	-13.292
12	1.44	-13.842	1.32	-13.879
13	1.54	-12.812	1.40	-12.854
14	2.29	-12.640	2.02	-12.694
15	5.47	-12.262	5.22	-12.282

## **APPENDICES REFERENCES**

## APPENDICES REFERENCES

1. Evans, R. B., J. H. DeVan, and G. M. Watson, Self-Diffusion of Chromium in Nickel-Based Alloys, ORNL-2982, (in press).
2. Redman, J. D., ORNL-2440, Classified, pp. 78-92 (1957).
3. DeVan, J. H., An Evaluation of Electro-Machining for the Analysis of Metal Surfaces, ORNL-CF-59-6-109 (1959).
4. Carslaw, H. S., and J. C. Jaeger, Conduction of Heat in Solids, p. 373. Oxford: University Press, 1950.
5. Evans, R. B., J. H. DeVan, and G. M. Watson, op. cit.

## VITA

The author, Jackson Harvey DeVan, was born on June 29, 1930, in Geneva, Illinois. He attended secondary schools in Geneva and Wheaton, Illinois, and was graduated from Wheaton Community High School in 1948. He then completed four years of undergraduate studies at Stanford University, Stanford, California, where in 1952 he received a Bachelor of Science Degree in Metallurgical Engineering, graduating cum laude. Upon graduation, the author was commissioned a Second Lieutenant in the United States Air Force and served from 1952 to 1954 as a project officer in the Materials Laboratory, Wright Air Development Center, Wright-Patterson Air Force Base, Ohio. While on duty with the Air Force, he completed twenty hours of graduate study at Ohio State University, Columbus, Ohio. In 1954 the author accepted a position as metallurgist with the Metallurgy Division of Oak Ridge National Laboratory. At present he is group leader of the Corrosion Engineering Group of the Metallurgy Division. He resides in Oak Ridge, Tennessee, with his wife, Margaret, whom he married in 1950, and his three children.

The author enrolled at the University of Tennessee Graduate School Extension at Oak Ridge in the Fall Quarter of 1954. He completed all his course work in Oak Ridge and performed his thesis work at the Oak Ridge National Laboratory.